

# Ladder Operator Block-Encoding

William A. Simon,<sup>1</sup> Carter M. Gustin,<sup>1</sup> Kamil Serafin,<sup>1</sup> Alexis Ralli,<sup>1</sup> Gary R. Goldstein,<sup>1</sup> and Peter J. Love<sup>1</sup>

<sup>1</sup>*Department of Physics and Astronomy, Tufts University, Medford, MA 02155, USA\**

(Dated: March 17, 2025)

We describe and analyze LOBE (Ladder Operator Block-Encoding), a framework for block-encoding second-quantized ladder operators that act upon fermionic and bosonic modes. We numerically benchmark these constructions using models arising in quantum field theories including the quartic oscillator, and  $\phi^4$  and Yukawa Hamiltonians on the light front. These benchmarks show that LOBE produces block-encodings with fewer non-Clifford operations, fewer block-encoding ancillae and overall number of qubits, and lower rescaling factors for various second-quantized operators as compared to block-encoding frameworks that expand the ladder operators in the Pauli basis. The LOBE constructions also demonstrate favorable scaling with respect to key parameters, including the maximum occupation of bosonic modes, the total number of fermionic and bosonic modes, and the locality of the operators. LOBE is implemented as an open source python package to enable further applications.

## I. INTRODUCTION

The simulation of many-body quantum systems is a promising application for future quantum computers. Following the original suggestion of Feynman [1], many general early algorithms were proposed [2–5]. Subsequently detailed proposals were developed for applications in specific areas, particularly quantum chemistry [6–10] and simulation of quantum field theories [11, 12]. Quantum simulation is now a broad area, with well developed algorithms for many applications [13–15].

In digital quantum simulation, quantum algorithms are composed using a series of unitary operations. Accessing the information of non-unitary operators - such as the Hamiltonian or other Hermitian observables of a quantum system - within a quantum algorithm is a necessary subroutine for conducting such simulations. This encoding task has been pursued through various means, resulting in methods such as Trotterization [16–20] and Block-Encoding [21–23].

Block-Encoding describes a general strategy for encoding a non-unitary matrix within a chosen subspace (block) of a larger unitary operator. Two general frameworks for constructing block-encodings of different operators - sparse block-encodings [21, 24, 25] and Linear Combinations of Unitaries (LCU) [26] - have allowed for the exploration of explicitly compiled block-encodings [27].

Quantum algorithms compiled into native gates give resource estimates that set targets for hardware development. With recent experimental demonstrations of quantum error correction [28, 29], establishing explicit resource estimates is important for establishing resource requirements for useful fault tolerant quantum computations.

Many previous works have numerically investigated various quantum simulation algorithms of purely

fermionic systems, with a particular emphasis on the simulation of molecules in quantum chemistry [9, 27, 30–36].

Another potential application of quantum computation are simulations of quantum field theories [12, 37–39], with specific applications in areas such as high-energy physics [15]. These systems often include interactions between fermions, antifermions, and bosons and several works have produced quantum resource estimates for simulating such systems [40–45]. In particular, Kirby et. al [40] detail simulation methods that use a compact-encoding scheme applied to second-quantized operators to produce near-optimal scaling for the required number of qubits to encode the system.

In this work, we detail a framework for constructing block-encodings of second-quantized operators, which we refer to as Ladder Operator Block-Encoding (LOBE). This framework is defined for the occupation number encoding and does not require the use of operator transformations that expand fermionic [46–48] and bosonic [49, 50] ladder operators in the Pauli operator basis. By directly block-encoding the operators in their second-quantized form, LOBE avoids the potential overhead caused by these operator transformations.

We provide numerical quantum resource estimates for implementing block-encodings of several classes of operators and different Hamiltonians that arise in quantum field theories, including various operators which model nontrivial interactions between fermionic, antifermionic, and bosonic modes. We analyze space-time quantum resources for LOBE - in comparison to techniques which require mapping ladder operators onto the Pauli basis - and find that LOBE results in constructions that require fewer quantum resources and show favorable scaling with respect to several parameters for many of the systems examined.

This work is organized as follows. In Section II, we review ladder operators in second quantization. In Section III, we review block-encodings and discuss frameworks for constructing block-encodings of different operators. In Section IV, we describe the LOBE framework, show

---

\* william.andrew.simon@gmail.com

compiled block-encodings for several classes of second-quantized operators, and give analytical space-time costs of the associated constructions. In Section V, we provide numerical quantum resource estimates for block-encodings of various classes of operators and Hamiltonians. In Section VI, we summarize the results presented in this work and discuss future directions.

## II. SECOND QUANTIZATION

Quantum operators in many-body quantum mechanics and quantum field theory are described in the framework of second quantization [51]. In second quantization, multiparticle states are written in terms of fermionic, antifermionic, and bosonic modes which can be occupied by different numbers of particles. The occupation number basis is defined by the product of occupation numbers of each of the respective modes:  $|n\rangle = |n_{I-1}, \dots, n_1, n_0\rangle$  where  $n_i$  is the number of particles in the  $i^{\text{th}}$  mode.

The space spanned by the occupation basis is called the *Fock space* ( $\mathcal{F}$ ) and the state vectors are referred to as *Fock states*. The Fock space is a direct sum of  $n$ -particle sectors [52]. In quantum field theories, field operators act on second-quantized states to create and annihilate particles in the field. This action is described in terms of ladder operators.

Ladder operators are quantum operators that act on fermionic, antifermionic, and bosonic modes to either increase (create) or decrease (annihilate) the number of particles occupying a particular mode. Many observables of interest for these systems, such as the Hamiltonian, can be efficiently expressed as sums or products of ladder operators.

### A. Bosonic Ladder Operators

Bosonic modes have no physical limitation on the occupancy of each mode, hence the Hilbert space of a single bosonic mode is countably infinite dimensional. The commutation rules for the bosonic annihilation ( $a_i$ ) and creation ( $a_i^\dagger$ ) operators are given by:

$$\begin{aligned} [a_i, a_j^\dagger] &= \delta_{ij} \\ [a_i, a_j] &= [a_i^\dagger, a_j^\dagger] = 0 \end{aligned} \quad (1)$$

Additionally, bosonic ladder operators commute with fermionic (and antifermionic) ladder operators.

For discretized computations, a cutoff on the bosonic occupancy ( $\Omega$ ) is chosen to make the dimension of the Hilbert space finite:  $\omega_i \in [0, 1, 2, \dots, \Omega]$ . The cutoff on the bosonic occupancy can introduce error as some physically allowable states become computationally inaccessible. Since there is no finite dimensional realization of the bosonic ladder operators, simulations of bosonic systems often proceed by increasing  $\Omega$  until the error induced by this cutoff is either negligible or well understood.

With the imposed bosonic cutoff, the action of bosonic creation operator ( $a_i^\dagger$ ) is defined by:

$$a_i^\dagger |\omega_i\rangle = \begin{cases} \sqrt{\omega_i + 1} |\omega_i + 1\rangle & \text{when } |\omega_i\rangle \neq |\Omega\rangle \\ 0 & \text{when } |\omega_i\rangle = |\Omega\rangle \end{cases} \quad (2)$$

where  $a_i^\dagger$  denotes a bosonic creation operator on the  $i^{\text{th}}$  mode,  $|\omega_i\rangle$  is the occupation of the  $i^{\text{th}}$  bosonic mode, and  $\Omega$  is the maximum number of bosons allowed in a single mode.

The action of the bosonic annihilation operator acting on the  $i^{\text{th}}$  mode ( $a_i$ ) with the imposed bosonic cutoff is defined by:

$$a_i |\omega_i\rangle = \begin{cases} \sqrt{\omega_i} |\omega_i - 1\rangle & \text{when } |\omega_i\rangle \neq |0\rangle \\ 0 & \text{when } |\omega_i\rangle = |0\rangle \end{cases} \quad (3)$$

### B. Fermionic Ladder Operators

Fermions (and antifermions) obey the Pauli-exclusion principle [53]. Therefore, fermionic (or antifermionic) occupation numbers are either 0 or 1. Fermionic ladder operators act on a single mode as:

$$b_i^\dagger |n_{i_b}\rangle = \begin{cases} p(n) |1\rangle & \text{when } |n_{i_b}\rangle = |0\rangle \\ 0 & \text{when } |n_{i_b}\rangle = |1\rangle \end{cases} \quad (4)$$

where  $b_i^\dagger$  denotes a fermionic creation operator on the  $i^{\text{th}}$  mode,  $|n_{i_b}\rangle$  is the occupation of the  $i^{\text{th}}$  fermionic mode in the Fock state, and  $p(n)$  denotes a potential sign flip described below.

The action of the fermionic annihilation operator is given by:

$$b_i |n_{i_b}\rangle = \begin{cases} p(n) |0\rangle & \text{when } |n_{i_b}\rangle = |1\rangle \\ 0 & \text{when } |n_{i_b}\rangle = |0\rangle \end{cases} \quad (5)$$

where  $b_i$  denotes a fermionic annihilation operator on the  $i^{\text{th}}$  mode

For a fermionic creation operator, if the mode being acted upon is unoccupied, then the creation operator “creates” a fermion in that mode. If the mode is already occupied before the creation operator is applied, then the operator sets the amplitude of the quantum state to zero. The action of the annihilation operators is opposite to that of the creation operators. If the mode is unoccupied before the operator is applied, then the annihilation operator sets the amplitude of the state to zero. If the mode is already occupied, then the annihilation operator “annihilates” the fermion in that mode by updating the mode to be unoccupied.

The potential sign flip caused by the fermionic ladder operators,  $p(n)$ , is determined by the parity of the occupation of the preceding modes:

$$p(n) = (-1)^{\sum_{j < i} n_{j_b}} \quad (6)$$

If the number of occupied fermionic modes with index  $j < i$  is odd, then the sign of the output state is flipped.

The fermionic ladder operators can be reordered arbitrarily with the introduction of additional terms due to the following anticommutation rules:

$$\begin{aligned} \{b_i, b_j^\dagger\} &= \delta_{ij} \\ \{b_i, b_j\} &= \{b_i^\dagger, b_j^\dagger\} = 0 \end{aligned} \quad (7)$$

where  $\{\}$  denotes the anticommutator. The actions outlined in Equations 4 and 5 obey these anticommutation rules.

In addition to fermions, antifermions are often included in quantum field theories. The properties and commutation rules for antifermions are the same as fermions and the sign flip for antifermions includes the parity of the occupation of the fermionic modes. Therefore, for simplicity we will treat antifermionic modes simply as fermionic modes that are indexed after all native fermionic modes for the remainder of this work [54].

### C. Observables

Observables can be expressed as linear combinations of products of ladder operators acting on both fermionic and bosonic modes.

Normal ordering is a convention for expressing products of ladder operators wherein all creation operators appear to the left of all annihilation operators.

In this work, we will default to expressing operators in their *mode ordered* form. We say an operator ( $O$ ) is *mode ordered* when all ladder operators acting on a single mode are grouped next to one another and normal ordered:

$$O = \left( \prod_i (b_i^\dagger)^{\delta_{b_i^\dagger}} (b_i)^{\delta_{b_i}} \right) \left( \prod_{i'} (a_{i'}^\dagger)^{R_{i'}} (a_{i'})^{S_{i'}} \right) \quad (8)$$

where  $i$  and  $i'$  index the fermionic and bosonic modes respectively,  $\delta$  takes the value 0 or 1 to denote if the individual ladder operator is included in the term, and the values  $R_i$  and  $S_i$  are integers in the range  $[0, \Omega]$  which denote the exponent of the bosonic ladder operators acting on the  $i^{\text{th}}$  bosonic mode.

Any term may be normal ordered or mode ordered using the commutation rules (Eq. 1 and Eq. 7). In general, this will introduce more terms when reordering, e.g.,  $a_i a_i^\dagger = a_i^\dagger a_i + 1$ .

The ladder operator basis gives a natural basis for expressing many operators relevant to quantum systems. We refer to operators written in the basis of ladder operators as second-quantized operators.

## III. BLOCK-ENCODING

Digital quantum algorithms are composed of a sequence of unitary operators. However, it is often neces-

sary to access information about various non-unitary operators within a quantum algorithm. ‘‘Block-Encoding’’ refers to an access model where the information regarding non-unitary operators is encoded in a labeled subspace (block) of a larger unitary operator [26, 55].

If  $A$  represents some  $N_A \times N_A$  non-unitary matrix, then a block-encoding of  $A$  in matrix form is given by:

$$U_A = \begin{pmatrix} \bar{A} & * \\ * & * \end{pmatrix} \quad (9)$$

where  $U_A$  is a unitary operator,  $\bar{A}$  is a rescaled form of  $A$  such that the eigenvalues of  $U_A$  have magnitude 1, and matrix entries  $*$  denote matrix elements that ensure  $U_A$  is unitary.

The action of  $U_A$  on an arbitrary quantum state ( $|\psi\rangle$ ) with dimension  $N_A$  tensored with an ancilla register beginning in the all-zero state can be defined as:

$$U_A |\psi\rangle |0\rangle_{\text{anc}} = \bar{A} |\psi\rangle |0\rangle_{\text{anc}} + \beta_\psi |\perp\rangle \quad (10)$$

where  $|\phi\rangle_{\text{anc}}$  is a register of block-encoding ancillae used to generate  $U_A$ ,  $|\perp\rangle$  is a normalized quantum state that is orthogonal to any state in the encoded subspace, and  $\beta_\psi$  is a complex coefficient. In the above equations, the encoded subspace of the block-encoding is chosen (without loss of generality) to be the subspace where all block-encoding ancillae are in the zero state ( $|0\rangle$ ). This choice of the encoded subspace is assumed for all block-encodings in this work.

It is important to note that  $\beta_\psi$  is dependent on the initial state of the system register ( $|\psi\rangle$ ). The dependence of  $\beta$  on  $|\psi\rangle$  can be seen in a simple case where  $|\psi\rangle$  is an eigenstate of  $\bar{A}$ . If  $|\gamma_k\rangle$  is an eigenstate of  $A$  with eigenvalue  $k$  (where  $|k| < 1$  such that  $U_A$  can be made unitary), then Eq. 10 leads to:

$$U_A |\gamma_k\rangle |0\rangle_{\text{anc}} = k |\gamma_k\rangle |0\rangle_{\text{anc}} + \sqrt{1 - |k|^2} |\perp\rangle \quad (11)$$

where  $\sqrt{1 - |k|^2}$  is clearly dependent upon the eigenvalue associated with the eigenstate.

One way to interpret the action of the block-encoding operator ( $U_A$ ) of a matrix ( $A$ ) is that it produces a probabilistic application of the rescaled matrix ( $\bar{A}$ ). After the block-encoding is applied, if a measurement of the block-encoding ancillae results in all of those qubits being in the zero state, then  $\bar{A}$  has been applied to the quantum state. The probability for this measurement result to occur is given by  $\|\bar{A} |\psi\rangle\|^2$ .

The rescaling factor ( $\lambda$ ) of a block-encoding is given by:

$$A = \lambda \bar{A} \quad (12)$$

This rescaling factor can have important implications for the cost of quantum algorithms. Smaller rescaling factors generally lead to more efficient algorithms though the exact impact on the cost is algorithm-dependent. For example, the success probability of applying  $\bar{A}$  as described

above can decrease as  $\lambda$  increases. If the block-encoding is used to construct a quantum walk operator [22, 23] and used in Quantum Phase Estimation [22, 27, 34], then the output eigenvalue estimates are scaled by the rescaling factor which will affect both the error and the precision of the estimated value.

In the following Subsections, we will describe some commonly used frameworks for constructing block-encodings of different operators. In particular, we discuss both the Sparse-Oracle and Linear Combination of Unitaries (LCU) frameworks for generating block-encodings. Then we discuss methods to combine block-encodings of operators to produce block-encodings for a linear combination of operators or a product of operators.

### A. Sparse-Oracle Framework

The Sparse-Oracle framework [24, 25, 56–60] assumes the presence of oracles that provide both the location and the values of the nonzero matrix elements. In this Subsection, we primarily follow the description of this framework given by Lin [21].

When an operator is sparse within some known basis, the Sparse-Oracle framework can use this structure to reduce the cost of the block-encoding construction. Despite the use of the word “oracle”, a method for generating quantum circuits that implement the required oracles for general matrices is given in [41, 61]. Several works have explored explicitly compiled Sparse-Oracle block-encodings for particular systems [42, 61, 62].

Let  $A$  be an  $s$ -sparse matrix, such that  $A$  has a maximum of  $s$  nonzero entries in a single row and each matrix element ( $A_{ij}$ ) is restricted to have magnitude  $\leq 1$ . A Sparse-Oracle block-encoding for the matrix  $A$  is defined in terms of three oracles:  $D_s$ ,  $O_A$ , and  $O_c$ .

The “diffusion operator” ( $D_s$ ) is defined by:

$$D_s |0^{\log_2 S}\rangle = \frac{1}{\sqrt{S}} \sum_{l=0}^{S-1} |l\rangle \quad (13)$$

where  $S = 2^{\lceil \log_2 s \rceil}$  and  $|0^{\log_2 S}\rangle$  is a block-encoding ancilla register that the diffusion operator acts on. This oracle can be implemented by a tensor product of Hadamards:  $H^{\otimes \log_2 S}$ .

The “column oracle” ( $O_c$ ) is defined by:

$$O_c |j\rangle |l\rangle = |j\rangle |c(j, l)\rangle \quad (14)$$

where  $c(j, l)$  is a function that returns the row-index of the  $l^{\text{th}}$  nonzero matrix element in the  $j^{\text{th}}$  column.

Lastly, the “value oracle” ( $O_A$ ) is defined by:

$$O_A |0\rangle |j\rangle |i\rangle = (A_{ij} |0\rangle + \beta_{ij} |1\rangle) |j\rangle |i\rangle \quad (15)$$

where  $\beta_{ij} \equiv \sqrt{1 - |A_{ij}|^2}$ .

With these three oracles, a block-encoding for  $A$  is given by:

$$U_A = D_s O_c O_A D_s \quad (16)$$

Simple proofs that  $U_A$  block-encodes  $A$  are given in Camps et. al [41] and Gilyén et. al [60].

The rescaling factor of the block-encoding created by the form above is given by:

$$\lambda_{\text{SO}} = 2^{\log_2 S} \max_{ij} |A_{ij}| \quad (17)$$

where the factor of  $2^{\log_2 S}$  comes from the diffusion operator and is limited by the sparsity of  $A$  and the factor of  $\max_{ij} |A_{ij}|$  comes from the constraint that all matrix elements ( $A_{ij}$ ) are restricted to have magnitude  $\leq 1$ .

If  $s$  is not a power of two, then the rescaling factor can be reduced to  $\lambda_{\text{SO}} = 2^{\log_2 s} \max_{ij} |A_{ij}|$  by replacing the diffusion operator ( $D_s$ ) with the generalized *Uniform State Preparation* (USP) protocol which is discussed in more detail in Appendix B. Implementing USP typically requires more nontrivial operations than the diffusion operator, so a trade-off exists between reducing the rescaling factor and reducing the number of operations.

### B. Linear Combination of Unitaries Framework

An alternative framework proposed by Childs et. al [26] called Linear Combination of Unitaries (LCU) generates block-encodings of operators that can be written in the following form:

$$A = \sum_{l=0}^{L-1} \alpha_l U_l \quad (18)$$

where  $\alpha_l$  are positive, real-valued coefficients and each  $U_l$  is a unitary operator. The phase of an operator can be absorbed into the operator such that the coefficient is positive and real:  $-i\alpha_l U_l = \alpha_l (-iU_l)$ . A term with a complex coefficient can be treated as two distinct terms, each with a positive, real coefficient.

To generate an LCU block-encoding, two oracles, *Prepare* and *Select*, are required. LCU block-encodings also require a block-encoding ancilla register with  $\lceil \log_2 L \rceil$  qubits. This register is often referred to as the *index register* since the computational basis states of this register ( $|l\rangle$ ) index the  $L$  terms in Eq. 18.

The *Prepare* oracle maps the all-zero state of the index register to a particular superposition state that encodes the coefficients of the terms in the operator:

$$\text{Prepare: } |0^{\otimes \lceil \log_2 L \rceil}\rangle_{\text{index}} \rightarrow \sum_{l=0}^{L-1} \sqrt{|\alpha_l|/\lambda} |l\rangle_{\text{index}} \quad (19)$$

where  $\lambda$  is given by:

$$\lambda_{\text{LCU}} = \sum_{l=0}^{L-1} |\alpha_l| \quad (20)$$

The *Select* oracle applies the  $l^{\text{th}}$  unitary ( $U_l$ ) onto the system register when the index register is in the compu-

tation basis state  $|l\rangle$ :

$$\mathbf{Select}: \begin{cases} \text{Apply } U_l \text{ on } |\psi\rangle & \text{when } |\text{index}\rangle \text{ is } |l\rangle \text{ for } l < L \\ \text{Undefined} & \text{Otherwise} \end{cases} \quad (21)$$

and the *Select* oracle can apply any unitary for the computational basis states outside of the range  $[0, L)$ .

With these two oracles, a block-encoding for an operator  $A$  specified by Eq. 18 is given by:

$$U_A = (\mathbf{Prepare}^\dagger)(\mathbf{Select})(\mathbf{Prepare}) \quad (22)$$

with an overall rescaling factor of  $\lambda_{\text{LCU}}$  (Eq. 20). A proof that  $U_A$  block-encodes  $A$  is given in Section 7.3 of Lin [21].

### 1. Implementing *Prepare*

The matrix representation of the *Prepare* oracle in the computational basis is given by:

$$\mathbf{Prepare} = \begin{bmatrix} \sqrt{|\alpha_0|/\lambda_{\text{LCU}}} & * & \dots & * \\ \sqrt{|\alpha_1|/\lambda_{\text{LCU}}} & * & \dots & * \\ \vdots & \vdots & \ddots & \vdots \\ \sqrt{|\alpha_{L-1}|/\lambda_{\text{LCU}}} & * & \dots & * \end{bmatrix} \quad (23)$$

From this definition, it is clear that there are infinitely many unitaries that implement the *Prepare* oracle since only the first column of the operator is fixed.

The *Prepare* oracle is a state preparation routine where the target state is a specific superposition state that encodes a probability distribution along the computational basis states. Many state preparation algorithms exist, however, the Grover-Rudolph algorithm [63] is a state preparation algorithm designed for target states of this form (Eq. 19). The cost of implementing Grover-Rudolph scales exponentially with the number of qubits in the register it acts upon. Since the size of the index register is logarithmic in the number of terms ( $L$ ), the number of operations required to implement Grover-Rudolph is linear in  $L$ . A more detailed discussion of the Grover-Rudolph state preparation algorithm is given in Appendix G.

For operators that have structure among the coefficients of the terms, implementations of *Prepare* can be constructed that leverage this structure to reduce the number of operations required to implement the oracle. In certain cases, this can drastically reduce the cost, for example for the Fermi-Hubbard model in [27].

### 2. Implementing *Select*

The *Select* oracle for an operator  $A$  as defined by Eq. 18 can be implemented by the operator:

$$U_{\text{Select}} = \sum_{l=0}^{L-1} |l\rangle \langle l| \otimes U_l + \sum_{l \geq L} |l\rangle \langle l| \otimes \mathbb{1} \quad (24)$$

Here we take the action of  $U_{\text{Select}}$  to be the identity operator for computational basis states of the index register outside the range  $[0, L)$ . However, if this constraint is relaxed or if there is structure in the description of the operator, then a more efficient implementation of *Select* can be constructed as in [27].

As an aside, if the implementation of the *Select* oracle is self-inverse, then the LCU block-encoding is also self-inverse. The construction for *Select* in Eq. 24 is naturally self-inverse if the unitaries themselves are self-inverse, which is true when the operator is decomposed in the Pauli basis. This structure makes LCU block-encodings particularly well-suited for being applied in algorithms based on Qubitization [23].

### C. Block-Encoding Linear Combinations of Non-Unitary Operators

A natural question to ask is if the structure of an LCU block-encoding can be generalized to a linear combination of non-unitary operators:

$$A = \sum_{l=0}^{L-1} \alpha_l O_l \quad (25)$$

where  $O_l$  are operators and we again restrict the coefficients  $\alpha_l$  to be positive and real-valued without loss of generality.

Following Gilyén et. al [60], an operator of this form (Eq. 25) can be block-encoded using an LCU block-encoding of a linear combination of unitary operators ( $U_l$ ) that each block-encode the operators  $O_l$ .

Let the set of unitary operators  $\{U_l\}$  represent block-encodings of the operators  $O_l$ :

$$U_l |\psi\rangle |0\rangle_{\text{anc}} = \bar{O}_l |\psi\rangle |0\rangle_{\text{anc}} + \beta_{\psi,l} |\perp\rangle \quad (26)$$

where each block-encoding uses the same encoded subspace and has a rescaling factor  $\lambda_l$  such that  $\lambda_l \bar{O}_l = O_l$ . Additionally, let the operator  $\tilde{A}$  be defined by the linear combination of the block-encoding unitaries:

$$\tilde{A} = \sum_l \tilde{\alpha}_l U_l \quad \tilde{\alpha}_l = \frac{\alpha_l \lambda_l}{\Lambda} \quad (27)$$

where  $\Lambda \geq \max_l \lambda_l$ .

Then, an LCU block-encoding ( $U_{\tilde{A}}$ ) of  $\tilde{A}$  will also give a block-encoding of  $A$ . In this work, we will refer to a block-encoding of this form as a Linear Combination of Operators (LCO).

The fact that  $U_{\tilde{A}}$  block-encodes  $A$  can be seen from the linearity of the operators themselves:

$$\begin{aligned} U_{\tilde{A}} &= \begin{pmatrix} \tilde{A} & * \\ * & * \end{pmatrix} \propto \sum_l \begin{pmatrix} \tilde{\alpha}_l U_l & * \\ * & * \end{pmatrix} \\ &= \sum_l \begin{pmatrix} \left( \begin{pmatrix} \alpha_l O_l & * \\ * & * \end{pmatrix} \right) & * \\ * & * \end{pmatrix} \end{pmatrix} \quad (28) \end{aligned}$$

It is clear from this form that the block-encodings  $\{U_l\}$  must all act in the same subspace as they would otherwise not yield the desired linear combination in the encoded subspace of  $U_{\tilde{A}}$ . It is also worth noting that the block-encodings  $\{U_l\}$  may all use the same block-encoding ancillae as long as the implementation of the *Select* oracle ensures that the block-encoding ancillae begin in the all-zero state in the subspace in which each individual block-encoding unitary is applied.

The overall rescaling factor of an LCO block-encoding is given by:

$$\lambda_{\text{LCO}} = \sum_{l=0}^{L-1} |\tilde{\alpha}_l| \quad (29)$$

As noted by Jennings et. al [64], if  $\Lambda = \max_l \lambda_l$ , then the overall rescaling factor becomes:

$$\lambda_{\text{LCO}} = \sum_{l=0}^{L-1} |\alpha_l \lambda_l| \quad (30)$$

The spacetime cost of implementing an LCO block-encoding is similar to the cost of implementing an LCU block-encoding. The *Prepare* and *Select* oracles can be implemented as described in Subsection III B, however, one must account for the cost of implementing the block-encoding unitaries  $\{U_l\}$  when implementing *Select*. Additionally, if  $m$  is the maximum number of block-encoding ancillae used for the block-encoding unitaries  $\{U_l\}$ , then an LCO block-encoding requires at least  $m + \lceil \log_2 L \rceil$  block-encoding ancillae.

As noted in prior works [21, 57, 59, 60, 64], an LCO can be thought of as a generalization of LCU to produce a block-encoding for a linear combination of matrices. Alternatively, it may be enlightening to consider an LCU block-encoding as a special case of an LCO block-encoding wherein the operators in the linear combination are all unitary and thus block-encode themselves.

#### D. Block-Encoding Products of Non-Uniatry Operators

It is natural to ask if a block-encoding for a product of operators can be easily produced, assuming access to block-encodings for the individual operators. As noted by Gilyén et. al [60], a block-encoding for a product of operators can be constructed by the product of the block-encodings of the individual operators.

Let  $A$  represent a product of operators  $B$  and  $C$ :

$$A = BC \quad (31)$$

with block-encodings  $U_B$  and  $U_C$ . Then, the product of  $U_B$  and  $U_C$  results in a block-encoding of  $A$ :

$$\begin{aligned} U_B U_C |\psi\rangle |0\rangle_{\text{anc},C} |0\rangle_{\text{anc},B} = \\ U_B (\bar{C} |\psi\rangle |0\rangle_{\text{anc},C} + \beta_{\psi,C} |\perp^*\rangle) |0\rangle_{\text{anc},B} = \\ \bar{B} \bar{C} |\psi\rangle |0\rangle_{\text{anc},C} |0\rangle_{\text{anc},B} + \beta_{\psi,C,B} |\perp\rangle \end{aligned} \quad (32)$$

with an overall rescaling factor of  $\lambda = \lambda_B \lambda_C$ .

It is important to note that in general the block-encodings for the individual operators ( $U_B$  and  $U_C$ ) require separate block-encoding ancillae. This constraint ensures that each block-encoding unitary acts on an ancilla register beginning in the all-zero state to adhere to the form of Eq. 10.

A block-encoding of this form can be generated for any operator,  $A$ , given by a product of  $L$  operators with individual block-encodings  $\{U_l\}$ . The number of operations for a block-encoding of this form is simply the sum of the operations required for each individual block-encoding unitary,  $\{U_l\}$ . The total number of block-encoding ancillae required is the sum of the number of block-encoding ancillae required for the individual block-encodings. The overall rescaling factor is the product of rescaling factors of the individual block-encoding unitaries, which will scale exponentially with the number of operators in the product.

## IV. COMPILING LADDER OPERATOR BLOCK-ENCODINGS

In this Section, we provide a framework for compiling controlled block-encodings of products and linear combinations of fermionic and bosonic ladder operators. The compilations presented below are optimized primarily to reduce the number of non-Clifford operations and secondarily to reduce the number of block-encoding ancillae at the expense of “clean ancillae”. Clean ancillae refer to ancilla qubits that are used temporarily in a computation such that they begin and end in the zero-state and can be reused on subsequent operations.

Although controlled applications of block-encodings are not always required in quantum algorithms, control qubits are included throughout this Section to demonstrate that controlling the block-encoding does not significantly increase the cost. For applications that do not require a controlled application of the block-encoding, the control qubits can simply be omitted and the cost associated with the uncontrolled block-encoding will be reduced accordingly.

### A. Encoding

The Jordan-Wigner transformation [46] maps fermionic ladder operators to Pauli operators acting on qubits. Under this transformation, the occupation states of fermionic modes are represented by qubit states using the following map:

$$|n_{I_b-1} \dots n_{1_b} n_{0_b}\rangle \rightarrow |q_{I_b-1} \dots q_{1_b} q_{0_b}\rangle \quad (33)$$

where  $I_b$  is the number of fermionic modes and  $n_{i_b} = q_{i_b} \in [0, 1]$  depending on if the  $i^{\text{th}}$  fermionic mode is occupied ( $|1\rangle$ ) or unoccupied ( $|0\rangle$ ). In this work, we use

the Jordan-Wigner encoding to represent the occupation states of fermionic modes. The number of qubits required for the fermionic system is equal to the number of fermionic modes.

The encoding scheme for bosons must be able to represent a number of bosons in the range  $\omega_i \in [0, \Omega_i]$  for each bosonic mode. In this work, we assume that the maximum bosonic occupancy for each bosonic mode is identical ( $\Omega_i = \Omega$ ). However, this encoding scheme and the block-encoding constructions presented below can be adapted to allow for bosonic modes with different bosonic cutoffs.

We choose to represent the occupancy of a bosonic mode in the binary encoding following [43]. In the binary encoding, the number of qubits needed to represent each mode is  $W = \lceil \log_2(\Omega + 1) \rceil$ .

Fock basis states that include the occupation of multiple fermionic and bosonic modes can be expressed as tensor products of the occupation states of the individual modes:

$$\begin{aligned} |n\rangle &\rightarrow |n_{I_b-1}\rangle \otimes \dots \otimes |n_0\rangle \otimes |\omega_{I_a-1}\rangle \otimes \dots \otimes |\omega_0\rangle \\ &\rightarrow |q_{I_b-1}\rangle \otimes \dots \otimes |q_0\rangle \otimes |q_{I_a-1}^{W-1} \dots q_{I_a-1}^1 q_{I_a-1}^0\rangle \otimes \\ &\quad \dots \otimes |q_0^{W-1} \dots q_0^1 q_0^0\rangle \end{aligned} \quad (34)$$

where  $I_a$  is the number of bosonic modes.

There are many alternative encoding schemes [40], including the Bravyi-Kitaev encoding [47, 48] for fermionic modes. Circuit constructions for these alternative encoding schemes could be considered, and we leave this for future work.

## B. Fermionic Ladder Operators

Here, we construct block-encodings for the individual fermionic creation ( $b_j^\dagger$ ) and annihilation ( $b_j$ ) operators. As these are block-encodings of non-unitary operators, we define the associated unitary operators as in Eq. 10:

$$U_{b_j^\dagger} |n_j\rangle |0\rangle_{\text{anc}} = b_j^\dagger |n_j\rangle |0\rangle_{\text{anc}} + \beta |\perp\rangle \quad (35)$$

The L2 norm of the fermionic ladder operators in the Fock basis is 1. Therefore these operators do not need to be rescaled.

The definition of the fermionic creation operator (Eq. 4) results in two implications. If the mode is *unoccupied*, then the mode should become occupied and a potential phase flip - determined by the occupancy of the preceding fermionic modes - should be applied. If the mode is occupied, then state should be modified to have zero amplitude in the encoded subspace. Therefore, the non-trivial action of the unitary will be dependent on the occupation of the associated fermionic mode:

$$U_{b_j^\dagger} |n_j\rangle |0\rangle_{\text{anc}} = \begin{cases} p(n) |1\rangle |0\rangle_{\text{anc}} & \text{when } |n_j\rangle \text{ is } |0\rangle \\ |\perp\rangle & \text{when } |n_j\rangle \text{ is } |1\rangle \end{cases} \quad (36)$$

where  $p(n)$  denotes the potential phase flip induced by the parity of the occupation of the preceding fermionic modes as defined by Eq. 6.

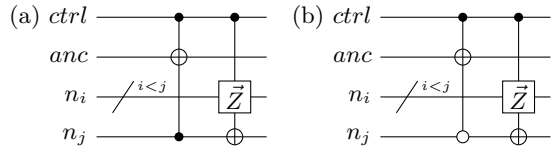


FIG. 1. **Fermionic Ladder Operator Block-Encodings**

In (a), a block-encoding for the fermionic creation operator acting on the  $j^{\text{th}}$  mode is given. In (b), a block-encoding for the fermionic annihilation operator acting on the  $j^{\text{th}}$  mode is given. For a creation (annihilation) operator, the branch of the wavefunction will be flipped outside of the encoded subspace if the mode is occupied (unoccupied). The state is updated by applying Pauli  $Z$  gates to the preceding fermionic modes which result in the output state having the appropriate sign based on  $p(n)$ . Then a Pauli  $X$  gate is applied to flip the occupation of the  $j^{\text{th}}$  mode.

An implementation for  $U_{b_j^\dagger}$  is given in Subfigure 1a. The initial Toffoli gate flips the ancilla qubit to indicate that the state is entirely outside of the encoded subspace when the control qubit is on ( $|1\rangle$ ) and the fermionic mode is occupied ( $|1\rangle$ ). The sign of the output state corresponding to  $p(n)$  can be applied appropriately using a series of controlled Pauli  $Z$  operators applied to each of the fermionic modes with index  $i < j$ :  $\bar{Z}_i$ . The occupation of the fermionic mode on which the ladder operator acts is updated using a controlled Pauli  $X$  operator:  $X_j$ .

A block-encoding for the fermionic annihilation operator,  $U_{b_j}$ , can be constructed similarly to  $U_{b_j^\dagger}$  and is shown in subfigure 1b. The fermionic creation operator ( $b^\dagger$ ) only acts nontrivially when the mode it acts upon is *unoccupied*. Inversely, the fermionic annihilation operator ( $b$ ) will only act nontrivially if the mode it acts upon is *occupied*. Therefore, the block-encoding ancilla is flipped outside of the encoded subspace if the control qubit is on ( $|1\rangle$ ) and the fermionic mode is unoccupied ( $|0\rangle$ ).

Each Toffoli gate can be implemented with four  $T$  gates using one clean ancilla [65, 66]. Likewise, an  $N$ -controlled Toffoli gate acting on a clean ancilla can be decomposed into a series of Toffoli gates acting on several clean ancillae [67]. The space-time costs for these decompositions are discussed in more detail in Appendix C. Throughout the remainder of this Section, we will assume these strategies are used to implement Toffoli gates.

In total, these block-encoding circuits have a rescaling factor of  $\lambda = 1$ , require one block-encoding ancilla and one clean ancillae, and use four  $T$  gates.

## C. Products of Fermionic Ladder Operators

In this Subsection, we construct block-encodings for a product of fermionic ladder operators. These construc-

tions use fewer quantum resources than would be required by combining the block-encodings of the individual operators using the strategy outlined in Subsection III D.

We define the number of “active modes” as the number of unique modes upon which an operator is applied nontrivially. For example, the operator  $b_i b_j^\dagger b_k b_l^\dagger$  has 4 active modes:  $i, j, k, l$ . We will use  $B$  to represent the number of active modes in a given operator.

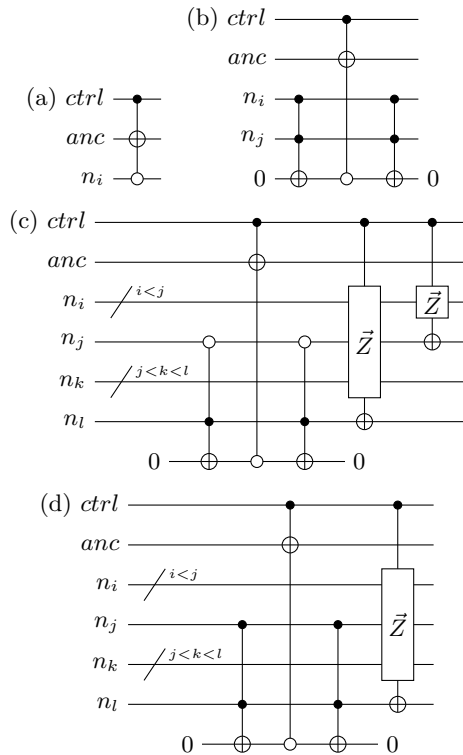


FIG. 2. **Block-Encoding Products of Fermionic Ladder Operators** In (a), a block-encoding for the fermionic number operator acting on the  $i^{\text{th}}$  mode ( $b_i^\dagger b_i$ ) is given. In (b), a block-encoding for the product of two fermionic number operators acting on the  $i^{\text{th}}$  and  $j^{\text{th}}$  modes ( $b_i^\dagger b_i b_j^\dagger b_j$ ) is given. In (c), a block-encoding for the operator  $b_j^\dagger b_l$  with  $j \neq l$  is given. In (d), a block-encoding for the operator  $b_j^\dagger b_j b_l$  with  $j \neq l$  is given.

Consider the action of the fermionic number operator ( $b_i^\dagger b_i$ ):

$$b_i^\dagger b_i |n_i\rangle = \begin{cases} |1\rangle & \text{when } |n_i\rangle \text{ is } |1\rangle \\ 0 & \text{when } |n_i\rangle \text{ is } |0\rangle \end{cases} \quad (37)$$

If the  $i^{\text{th}}$  mode is unoccupied, the state should have zero amplitude in the encoded subspace. If the  $i^{\text{th}}$  mode is occupied, then the state is left unchanged.

This action can be encoded using the circuit shown in Subfigure 2a. The Toffoli gate flips the block-encoding ancilla outside of the encoded subspace if the control is on and the  $i^{\text{th}}$  mode is unoccupied. Otherwise, the state

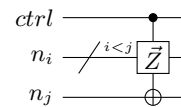


FIG. 3. **Block-Encoding Linear Combination of Fermionic Creation and Annihilation Operators** A block-encoding for the operator  $b_j + b_j^\dagger$  is given.

of the system and the block-encoding ancilla are left unchanged.

Block-encoding this operator as the product of the block-encodings for  $b_i$  and  $b_i^\dagger$  would require two block-encoding ancillae and use 8  $T$  gates. Meanwhile, this construction has a rescaling factor of  $\lambda = 1$ , requires one block-encoding ancilla and one clean ancilla, and uses four  $T$  gates.

A block-encoding circuit for the operator  $b_j^\dagger b_l$  is given in Subfigure 2c. For this operator, the amplitude of the state in the encoded subspace should be zero *unless* both the  $j^{\text{th}}$  mode is unoccupied and the  $l^{\text{th}}$  mode is occupied. If the control qubit is on and these two conditions are not both true, then the block-encoding ancilla is flipped outside of the encoded subspace. The state of the system is updated based on the two operators in the order in which they would act upon the quantum state:  $\vec{Z} X_l (b_l)$  then  $\vec{Z} X_j (b_j^\dagger)$ . This block-encoding circuit has a rescaling factor of  $\lambda = 1$ , requires one block-encoding ancilla and two clean ancillae, and uses 8  $T$  gates.

This construction can be generalized to an arbitrary product of ladder operators. Each active mode will contribute a new control condition on the state of the corresponding mode. A block-encoding circuit of this form for a general product of fermionic ladder operators with  $B$  active modes will have a rescaling factor of  $\lambda = 1$ , require one block-encoding ancilla and  $B$  clean ancillae, and use  $4B$   $T$  gates.

#### D. Linear Combinations of Fermionic Ladder Operators

In this Subsection, we show how to construct block-encodings of linear combinations of products of fermionic ladder operators. These constructions use fewer quantum resources than are required by the LCO construction described in Subsection III C. In particular, we give a generalized construction for a product of fermionic ladder operators plus its Hermitian conjugate, however, we note that the strategies we present here are not restricted to this case.

Consider a linear combination of an individual fermionic ladder operator with its Hermitian conjugate:  $b_j^\dagger + b_j$ . The action of this operator on the two possible



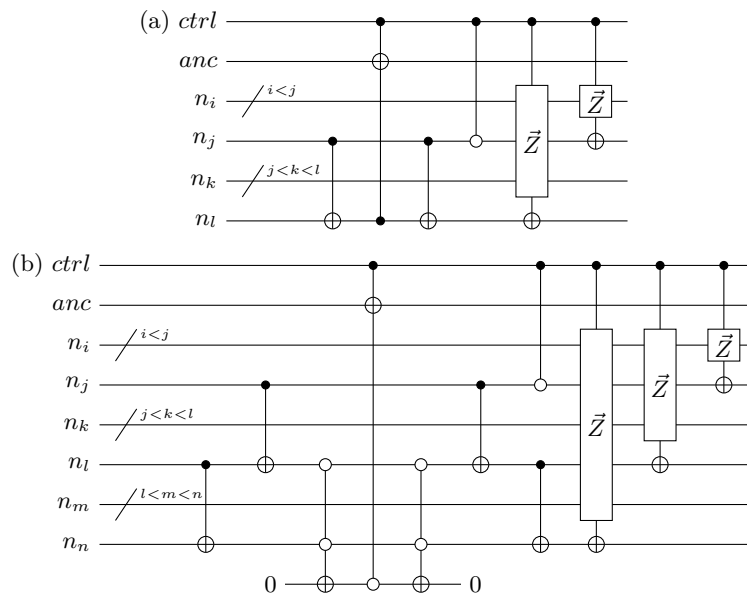


FIG. 4. **Block-Encoding Product of Fermionic Operators Plus Hermitian Conjugate** In (a), a block-encoding for the operator  $b_j b_l + b_l^\dagger b_j^\dagger$  is given. In (b), a block-encoding for the operator  $b_j b_l b_n + b_n^\dagger b_l^\dagger b_j^\dagger$  is given.

occupation states of the  $j^{\text{th}}$  fermionic mode is given by:

$$(b_j^\dagger + b_j) |n_j\rangle = \begin{cases} p(n) |1\rangle & \text{when } |n_j\rangle \text{ is } |0\rangle \\ p(n) |0\rangle & \text{when } |n_j\rangle \text{ is } |1\rangle \end{cases} \quad (38)$$

An LCO construction using the block-encodings for these two ladder operators presented in the previous Section would have a rescaling factor of  $\lambda = 2$ , require two block-encoding ancillae and two clean ancillae, and use 12  $T$  gates. However, by considering the action of this operator (Eq. 38) on the active mode, a more efficient block-encoding can be constructed. A Pauli  $X$  gate can be applied to the  $j^{\text{th}}$  mode to flip the occupation and a string of Pauli  $Z$  gates can be applied on each fermionic mode with index  $i < j$  to apply the potential phase flip induced by  $p(n)$ . This results in the same decomposition one would arrive at using the Jordan-Wigner transformation ( $\vec{Z}X_j$ ). A circuit diagram for this block-encoding is shown in Figure 3. This block-encoding circuit has a rescaling factor of  $\lambda = 1$ , requires zero block-encoding ancillae and zero clean ancillae, and uses zero non-Clifford operations.

For a two-body fermionic operator and its Hermitian conjugate ( $b_j b_l + b_l^\dagger b_j^\dagger$ ) with  $j \neq l$  we arrive at a construction that differs from the Jordan-Wigner transformation. We begin by swapping the operators in the second term using the anticommutation relations to ensure that the order in which the active modes appear in each term is the same:  $b_j b_l - b_l^\dagger b_j^\dagger$ . In the circuit, the order in which the system is updated based on the ladder operators is fixed so it must be consistent for both terms. This re-ordering means that the potential phase flips caused by each ladder operator will be consistent for both terms

since the order at which the operators are applied onto the system is consistent. The action of the joined operator on the possible occupation states of the  $j^{\text{th}}$  and  $l^{\text{th}}$  fermionic modes is given by:

$$(b_j b_l - b_l^\dagger b_j^\dagger) |n_l, n_j\rangle = \begin{cases} -p(n) |11\rangle & \text{when } |n_l, n_j\rangle \text{ is } |00\rangle \\ p(n) |00\rangle & \text{when } |n_l, n_j\rangle \text{ is } |11\rangle \\ 0 & \text{when } |n_l, n_j\rangle \text{ is } |01\rangle \\ 0 & \text{when } |n_l, n_j\rangle \text{ is } |10\rangle \end{cases} \quad (39)$$

It is clear that the action of this operator on the system is determined by the parity of the occupation of the two active fermionic modes.

In Subfigure 4a, we give a circuit diagram for block-encoding this two-body operator. The parity of the occupation of the active modes can be computed using a CNOT gate controlled on the  $j^{\text{th}}$  mode, targeting the  $l^{\text{th}}$  mode. If the control qubit is on and  $|n_l\rangle$  is in the  $|1\rangle$  state (odd parity), then the block-encoding ancilla is flipped to push that branch of the wavefunction outside of the encoded subspace. After this operation, the parity can be uncomputed, returning the qubit storing the occupation of the  $l^{\text{th}}$  mode to its original state. Next, a CZ gate that is 0-controlled on the  $j^{\text{th}}$  fermionic mode and 1-controlled on the control qubit applies the desired sign flip corresponding to the term  $-b_l^\dagger b_j^\dagger$ . Lastly, a series of  $\vec{Z}X$  operators are applied to each active mode in the order at which the operators would be applied onto the system (right to left).

For an operator of the form  $b_j b_l^\dagger + b_l b_j^\dagger$ , we can construct a similar block-encoding with a slight modification. In

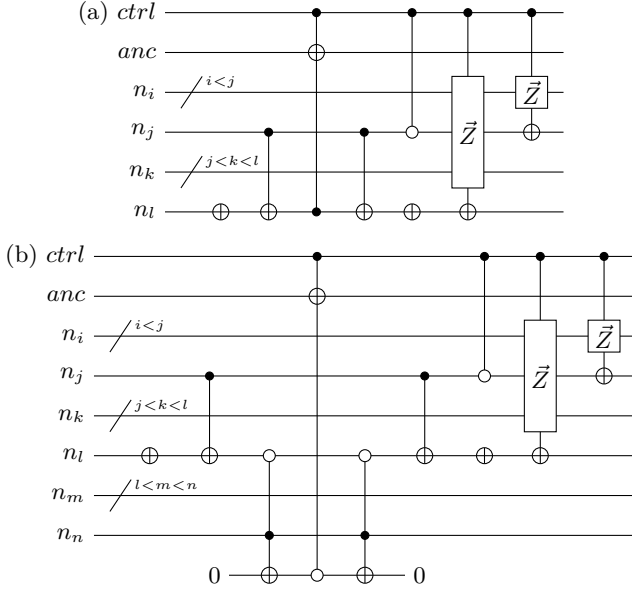


FIG. 5. **Block-Encoding Product of Fermionic Operators Plus Hermitian Conjugate (modifications)** In (a), a block-encoding for the operator  $b_j b_i^\dagger + b_i b_j^\dagger$  is given. In (b), a block-encoding for the operator  $b_j b_i^\dagger b_n^\dagger b_n + b_n^\dagger b_n b_i b_j^\dagger$  is given.

this case, we simply flip the occupation of the  $l^{\text{th}}$  mode using a Pauli  $X$  gate before we compute the parity of the modes. The circuit diagram for block-encoding this operator is given in Subfigure 5a.

Likewise, if a number operator is included in a term, this can be accounted for by including a 1-control on that mode when determining if the block-encoding ancilla should be flipped and excluding that mode from any parity computations. An example circuit diagram for an operator including a number operator is given in Subfigure 5b.

The construction of these block-encoding circuits can be generalized to any operator that is a product of fermionic operators plus its Hermitian conjugate. An example circuit diagram for this generalized construction is shown in Figure 6. If  $C$  represents the number of active modes excluding modes where a number operator is acting on the mode, then the  $CZ$  gate is present only if  $(C \bmod 2)$  is odd. These block-encoding circuits will all have rescaling factors of  $\lambda = 1$ , require one block-encoding ancilla and  $B - 1$  clean ancillae, and use  $4(B - 1)$   $T$  gates.

As mentioned, the strategy employed here to construct block-encodings of a linear combination of fermionic ladder operators is not restricted to the Hermitian case. Consider the action of the operator  $b_i b_j b_k^\dagger + b_j^\dagger b_i^\dagger b_k^\dagger$  on the occupation states of the fermionic modes. This operator will set the amplitude of the state in the encoded subspace to zero *unless* both  $|n_i \oplus n_j\rangle$  and  $|n_k\rangle$  are  $|0\rangle$ . The implementation of the block-encoding for this oper-

ator is given in Figure 7. This block-encoding circuit has a rescaling factor of  $\lambda = 1$ , requires one block-encoding ancilla and two clean ancillae, and uses 8  $T$  gates.

## E. Bosonic Ladder Operators

In this Section, we aim to define a family of unitaries that generate block-encodings of the bosonic creation ( $a_i^\dagger$ ) and annihilation ( $a_i$ ) operators. Based on the defined action of the bosonic creation operator (Eq. 2), a block-encoding unitary following the form of Eq. 10 can be defined as follows:

$$U_{a_i^\dagger} |\omega_i\rangle |0\rangle_{\text{anc}} = \begin{cases} \sqrt{\omega_i + 1/\Omega} |\omega_i + 1\rangle |0\rangle_{\text{anc}} + \beta |\perp\rangle & \text{when } \omega_i < \Omega \\ |\perp\rangle & \text{when } \omega_i \geq \Omega \end{cases} \quad (40)$$

where  $\omega_i$  is the occupation number of the  $i^{\text{th}}$  bosonic mode and the operator is rescaled by a factor of  $\sqrt{\Omega}$ .

The desired action of the block-encoding circuit for the bosonic creation operator is to increase the occupation of the bosonic mode by 1 and rotate the block-encoding ancilla such that it has a coefficient of  $\sqrt{\omega_i + 1/\Omega}$  in the  $|0\rangle$  state when the initial occupation of the  $i^{\text{th}}$  bosonic mode is  $\omega_i$ . This can be achieved by applying an incrementer circuit to the bosonic mode. An implementation of an incrementer circuit is shown in Figure 24, following the construction given by Gidney [68]. This incrementer increases the occupation by  $1 \bmod \Omega$  in each branch of the wavefunction. The desired amplitudes of the block-encoding ancilla can be obtained using a series of uniformly controlled  $R_y$  gates that are controlled on the corresponding bosonic occupation.

An example circuit diagram is given in Subfigure 8a. A block-encoding for the bosonic annihilation operator can be constructed similarly, but with the block-encoding ancilla rotated prior to the occupation of the mode being decremented (Subfigure 8b).

The angles of the  $R_y$  gates are determined classically by the following function:

$$\theta(\omega_i) = \begin{cases} 2 \cos^{-1} \left( \sqrt{\omega_i/\Omega} \right) & \text{when } \omega_i < \Omega \\ \pi & \text{when } \omega_i \geq \Omega \end{cases} \quad (41)$$

where  $\omega_i$  here in comparison with  $\omega_i + 1$  in Eq. 40 is due to the occupation of the state being updated prior to the controlled rotations. The value of  $\pi$  for the rotation angle sets the state of the block-encoding ancilla to be  $|\perp\rangle$ . This causes the amplitude of the state in the encoded subspace to be zero.

An implementation of a controlled incrementer circuit is given in [68] and depicted here in Figure 24. This implementation requires  $W - 1$  clean ancillae and  $3W$   $T$  gates. The series of uniformly controlled rotations can be decomposed via the protocol given in Möttönen

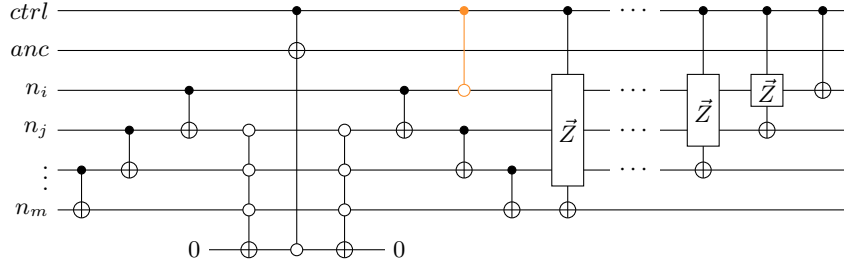


FIG. 6. **Generalized Block-Encoding for Product of Fermionic Operators Plus Hermitian Conjugate** A block-encoding for the operator  $b_i b_j \dots b_m + b_m^\dagger \dots b_j^\dagger b_i^\dagger$  is given. The  $CZ$  gate highlighted in orange is present only if the swapping on the order of the operators in the second term induces a negative sign on the second term (an odd number of swaps are required to reorder the ladder operators). Block-encodings for similar operators such as those that include number operators or different arrangements of the creation and annihilation operators can be accounted for using the modifications shown in Figure 5.

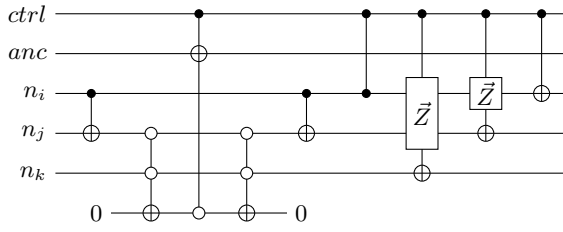


FIG. 7. **Block-Encoding for Linear Combination of Non-Conjugate Fermionic Operators** A block-encoding for the operator  $b_i b_j b_k^\dagger + b_j^\dagger b_i^\dagger b_k^\dagger$  is given.

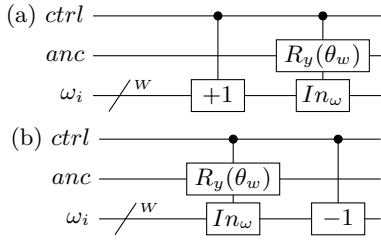


FIG. 8. **Bosonic Ladder Operator Block-Encoding** In (a), a block-encoding for the bosonic creation operator ( $a_i^\dagger$ ) is given. In (b), a block-encoding for the bosonic annihilation operator ( $a_i$ ) is given. The “+1” operation depicts an incrementer. The “-1” operation depicts a decrementer. The “ $In_\omega - R_y(\theta_w)$ ” operation depicts a series of uniformly controlled  $R_y$  rotations.

et. al [69]. A discussion of different schemes to construct a *controlled* set of uniformly controlled rotations is given in Appendix F. The resource estimates quoted in the remainder of this work assume the decomposition that requires (at most)  $\Omega + 3$  uncontrolled rotations and  $4\lceil \log_2 \Omega \rceil$   $T$  gates (Figure 29).

In total, this block-encoding has a rescaling factor of  $\lambda = \sqrt{\Omega}$ , requires one block-encoding ancilla and  $\lceil \log_2 \Omega \rceil$  clean ancillae, and uses  $7W$   $T$  gates and (at most)  $\Omega + 3$  arbitrary rotations.

## F. Products of Bosonic Ladder Operators

In this Subsection, we discuss constructing block-encodings for a product of bosonic ladder operators acting on the same mode. Unlike fermions, multiple bosons can occupy the same bosonic mode, and a series of bosonic ladder operators can be applied to the state. Products of bosonic ladder operators acting on different modes can be block-encoded using the methods described in Subsection III D.

Consider the desired action of a block-encoding for series of  $R$  bosonic creation operators acting on the  $i^{\text{th}}$  bosonic mode:

$$U_{(a_i^\dagger)^R} |\omega_i\rangle |0\rangle_{\text{anc}} = \begin{cases} f(\omega_i) |\omega_i + R\rangle |0\rangle_{\text{anc}} + \beta |\perp\rangle & \text{when } \omega_i \leq \Omega - R \\ |\perp\rangle & \text{when } \omega_i > \Omega - R \end{cases} \quad (42)$$

where

$$f(\omega_i) = \prod_{r=1}^R \sqrt{(\omega_i + r)/\Omega} \quad (43)$$

A block-encoding for this operator can be achieved by updating the occupation of the bosonic mode by  $+R$  and then performing a single series of rotations. A circuit diagram for this construction is shown in Subfigure 9a.

The angles of the  $R_y$  rotations are determined classically by the following function:

$$\theta(\omega_i, R) = \begin{cases} 2 \cos^{-1} \left( \prod_{r=0}^{R-1} \sqrt{(\omega_i - r)/\Omega} \right) & \text{when } \omega_i \leq \Omega - R \\ \pi & \text{when } \omega_i > \Omega - R \end{cases} \quad (44)$$

where  $\omega_i - r$  here in comparison with  $\omega_i + r$  in Eq. 42 is due to the occupation of the state being updated prior to the controlled rotations.

A block-encoding for a bosonic annihilation operator being applied  $S$  times can be achieved using a similar construction shown in subfigure 9b. The occupation of the

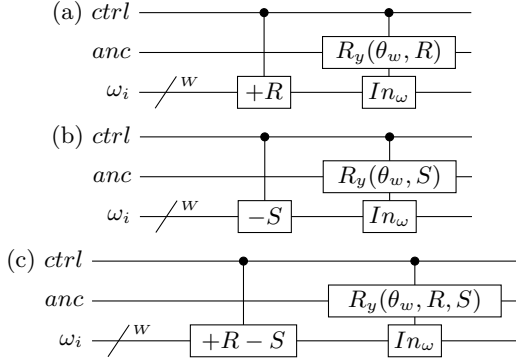


FIG. 9. **Block-Encoding Product of Bosonic Ladder Operators** In (a), a block-encoding for the operator  $(a_i^\dagger)^R$  is given. In (b), a block-encoding for the operator  $(a_i)^S$  is given. In (c), a block-encoding for the operator  $(a_i^\dagger)^R (a_i)^S$  is given. The “+ $R$ ” operation depicts an addition by the classical integer  $R$ . The “- $S$ ” operation depicts a subtraction by the classical integer  $S$ . The “ $In_\omega - R_y(\theta_\omega)$ ” operations depict series of uniformly controlled  $R_y$  rotations.

$$\theta(\omega_i, R, S) = \begin{cases} 2 \cos^{-1} \left( \left( \prod_{r=0}^{R-1} \sqrt{(\omega_i - r)/\Omega} \right) \left( \prod_{s=1}^S \sqrt{(\omega_i - R + s)/\Omega} \right) \right) & \text{when } S \leq \omega_i \leq \Omega - R \\ \pi & \text{Otherwise} \end{cases} \quad (46)$$

Incrementing a quantum register by a classical value can be implemented in multiple ways, with different implementations having different space-time tradeoffs. We discuss several different implementations for this operation in detail in Appendix D. The resource estimates presented in this work assume the compilation given in Figure 26, which requires (at most)  $3W$   $T$  gates [70]. In total, the block-encoding circuits shown in Figure 9 have a rescaling factor of  $\lambda = \Omega^{(R+S)/2}$ , require one block-encoding ancilla and  $\lceil \log_2 \Omega \rceil$  clean ancillae, and use (at most)  $7W$   $T$  gates and  $\Omega + 3$  arbitrary rotations.

### G. Linear Combinations of Bosonic Ladder Operators

In this Subsection, we construct block-encodings for the sum of a product of bosonic ladder operators with its Hermitian conjugate.

Consider the block-encodings for the operators  $a_i^\dagger$  and  $a_i$ . An efficient block-encoding of the operator  $a_i^\dagger + a_i$  can be constructed using the symmetry between the two individual block-encodings. To apply the creation operator, the occupancy is increased by 1 and then the rotations are applied, whereas for the annihilation operator, the rotations are applied first and then the occupancy is decreased by 1. Since the desired rotation angles are independent of which operator is being applied (Eq. 41), we can apply these rotations once for both opera-

mode is first decreased by  $S$  and then the uniformly controlled rotations are applied to pick up the corresponding coefficient on the block-encoding ancilla. The function to determine the rotation angles is given by:

$$\theta(\omega_i, S) = \begin{cases} 2 \cos^{-1} \left( \prod_{s=1}^S \sqrt{(\omega_i + s)/\Omega} \right) & \text{when } \omega_i \geq S \\ \pi & \text{when } \omega_i < S \end{cases} \quad (45)$$

Likewise, a block-encoding for an operator of the form  $(a_i^\dagger)^R (a_i)^S$  can be constructed using a similar form (subfigure 9c). The occupation of the mode is updated by a value of  $+R - S$  and then the uniformly controlled rotations are applied to pick up the corresponding coefficient on the block-encoding ancilla. The function to determine the rotation angles is given by:

tors. However, one additional block-encoding ancilla is required to index between the two operators. An example circuit diagram for this construction is shown in subfigure 10a. A block-encoding for the generalized operator  $((a_i^\dagger)^R (a_i)^S + (a_i^\dagger)^S (a_i)^R)$  can be constructed similarly and is shown in Subfigure 10b.

Likewise, this construction can be generalized to a linear combination of a product of bosonic operators acting on different modes plus its Hermitian conjugate. An example circuit diagram for this construction is shown in Figure 11. For an operator acting on  $B$  bosonic modes, these block-encodings have a rescaling factor of  $\lambda = 2\Omega^{P/2}$  where  $P$  is the sum of the exponents of the operators in a term:  $P = \sum_{b=0}^{B-1} (R_b + S_b)$ . Additionally, they require  $B+1$  block-encoding ancillae and  $\lceil \log_2 \Omega \rceil + 1$  clean ancillae, and use (at most)  $12BW - 8B + 4$   $T$  gates and  $B(\Omega + 3)$  arbitrary rotations.

### H. Terms with Fermionic and Bosonic Ladder Operators

In the previous Subsections, we discussed strategies for compiling block-encodings of different operators acting on either fermionic or bosonic modes. In this Subsection, we discuss block-encodings for operators that contain operators that act on both fermionic and bosonic operators.

Consider the action of the operator:  $b_i a_j + a_j^\dagger b_i^\dagger$  on

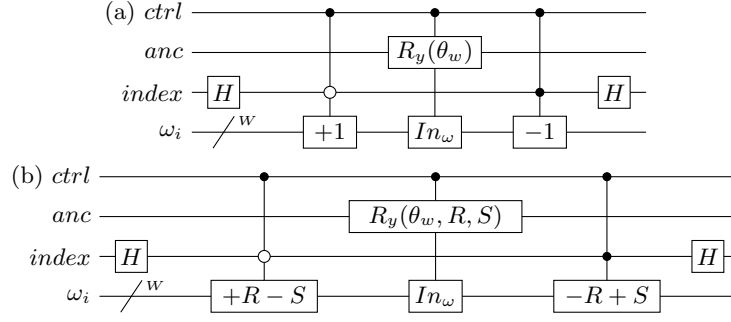


FIG. 10. **Block-Encoding Product of Bosonic Ladder Operators Plus Hermitian Conjugate** In (a), a block-encoding for the operator  $(a_i^\dagger + a_i)$  is given. In (b), a block-encoding for the operator  $((a_i^\dagger)^R (a_i)^S + (a_i^\dagger)^S (a_i)^R)$  is given.

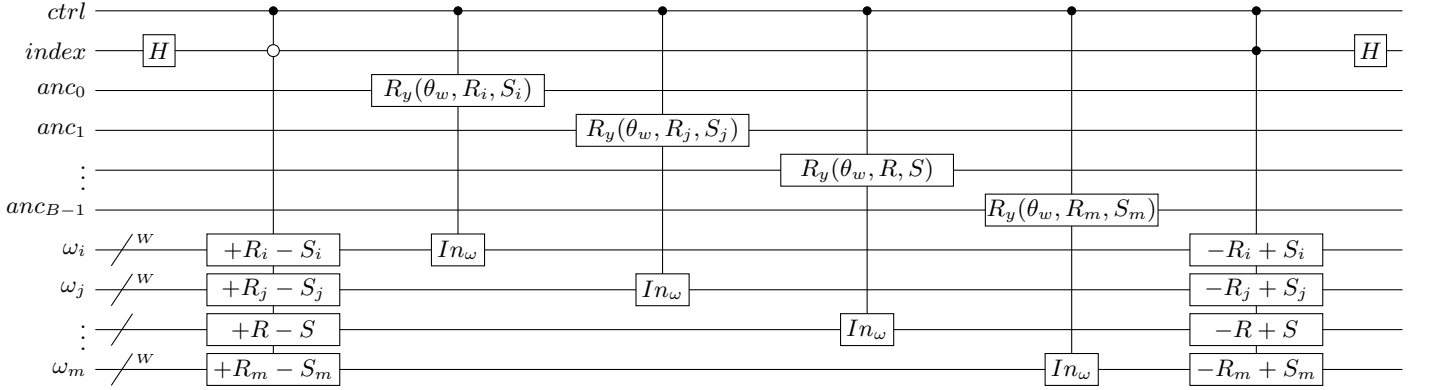


FIG. 11. **Generalized Block-Encoding Product of Bosonic Ladder Operators Plus Hermitian Conjugate** A block-encoding for the operator  $((a_i^\dagger)^{R_i} (a_i)^{S_i} (a_j^\dagger)^{R_j} (a_j)^{S_j} \dots (a_m^\dagger)^{R_m} (a_m)^{S_m} + h.c.)$  is given.

the respective fermionic and bosonic modes. When the fermionic mode is occupied, only the operator  $b_i a_j$  will act nontrivially. Meanwhile if the fermionic mode is unoccupied, only the operator  $a_j^\dagger b_i^\dagger$  will act nontrivially. Therefore, the occupation of the fermionic mode can be used to dictate which bosonic operator should be applied to the system. After the appropriate bosonic operator is applied, the fermionic system is updated. A circuit diagram for this block-encoding is given in subfigure 12a. This block-encoding circuit will have a rescaling factor of  $\lambda = \sqrt{\Omega}$ , requires one block-encoding ancilla and  $W + 1$  clean ancillae, and uses  $12W - 4$   $T$  gates and (at most)  $\Omega + 3$  arbitrary rotations.

This strategy can be employed for other combinations of bosonic and fermionic ladder operators. In Yukawa theory on the lightfront, the operator  $b_i^\dagger b_j^\dagger a_k + a_k^\dagger b_j b_i$  is used to model the process of a boson being annihilated to form a fermion-antifermion pair and a fermion-antifermion pair being annihilated to form a boson [54]. A block-encoding for this operator is shown in subfigure 12b. When constructing the circuit, the occupation of either fermionic mode can be used to determine which bosonic operator is applied to the system. This block-encoding circuit will have a rescaling factor of  $\lambda = \sqrt{\Omega}$ , requires two block-encoding ancillae and  $W + 1$  clean an-

cillae, and uses  $12W$   $T$  gates and (at most)  $\Omega + 3$  arbitrary rotations.

A similar block-encoding can be constructed for the operator  $b_i^\dagger b_j^\dagger a_k a_l + a_l^\dagger a_k^\dagger b_j b_i$ , which also appears in Yukawa theory on the lightfront [54]. An example circuit diagram for this block-encoding is shown in subfigure 12c. This block-encoding circuit will have a rescaling factor of  $\lambda = \Omega$ , requires three block-encoding ancillae and  $\lceil \log_2 \Omega \rceil + 1$  clean ancillae, and uses  $24W - 8$   $T$  gates and (at most)  $2\Omega + 6$  arbitrary rotations.

## V. RESULTS

In this Section, we numerically evaluate the quantum resources required for block-encoding various operators using LOBE. The space-time costs that we analyze include: the number of  $T$  gates, the number of non-Clifford single qubit rotations, the number of block-encoding ancillae, the maximum number of qubits required, and the rescaling factor imposed on the resulting block-encoding.

We compare the LOBE constructions presented in Section IV to techniques that first expand the ladder operators in the Pauli basis and then block-encode the resulting linear combinations of Pauli operators using LCU.

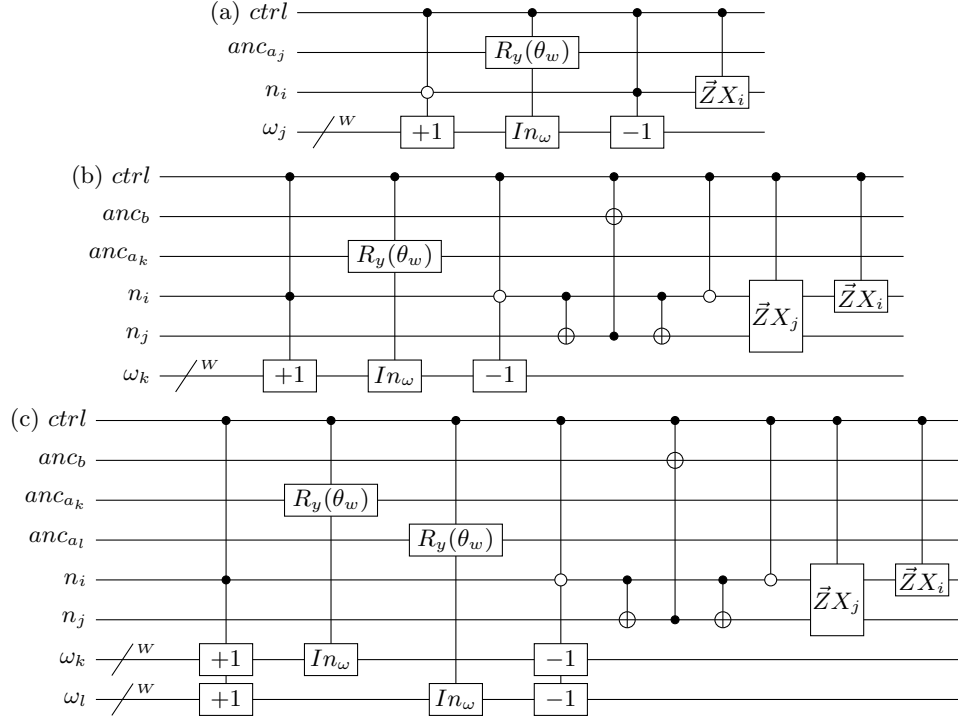


FIG. 12. **Block-Encoding Terms** In (a), a block-encoding for the operator  $b_i^\dagger a_j^\dagger + a_j b_i$  is given. In (b), a block-encoding for the operator  $b_i^\dagger b_j^\dagger a_k + a_k^\dagger b_j b_i$  is given. In (c), a block-encoding for the operator  $b_i^\dagger b_j^\dagger a_k a_l + a_l^\dagger a_k^\dagger b_j b_i$  is given.

The Jordan-Wigner transformation [46] is used to expand fermionic ladder operators in the basis of Pauli operators, while the Standard Binary encoding [50] is used to expand bosonic ladder operators.

The first Pauli-based method we compare against will be referred to as “Pauli Expansion”. In this method, the respective Pauli transformations are applied to all ladder operators within a term and the product is fully expanded. This results in a single linear combination of Pauli operators, which is then block-encoded using the LCU framework.

The second Pauli-based method we compare against will be referred to as “Piecewise Pauli”. In this method, each product of ladder operators acting on a single mode is expanded in the Pauli basis and then block-encoded using the LCU framework. These block-encodings of the ladder operators acting on each mode are then combined together to produce a block-encoding of the full operator using the techniques described in Subsections III C and III D.

In the following Subsections, we benchmark these three different block-encoding methods for various types of operators. First, we analyze the associated space-time costs for block-encoding several classes of operators which appear in many second-quantized models. These models include Hamiltonians derived from two non-relativistic models - the quartic harmonic oscillator [38, 39, 71] and the static massive Yukawa model [72] - and two fully relativistic models -  $\phi^4$  theory [73] and the massive Yukawa

model [74].

The results presented in this Section are generated using three open-source software libraries: LOBE [75], OpenParticle [76], and Symmer [77–80]. LOBE [75] provides methods to construct and validate block-encoding circuits, including those presented in this work. These circuits are implemented using Cirq [81] and are numerically verified for block-encodings of up to 18 qubits. OpenParticle is used to construct and manipulate the operators in terms of fermionic, antifermionic, and bosonic ladder operators. The Symmer software library is used for various subroutines, including expanding the ladder operators in the Pauli basis. The software library [82] is used to determine the rotation angles required for arbitrary state preparation using the Grover-Rudolph Algorithm [63].

## A. Components

In this Subsection, we numerically benchmark the space-time cost of LOBE constructions for three different sets of operators. We compare the cost of the LOBE constructions with the Pauli Expansion construction and the Piecewise Pauli construction described in Subsection V.

The first set of operators we examine are described by a product of fermionic annihilation operators acting on different modes plus its Hermitian conjugate:

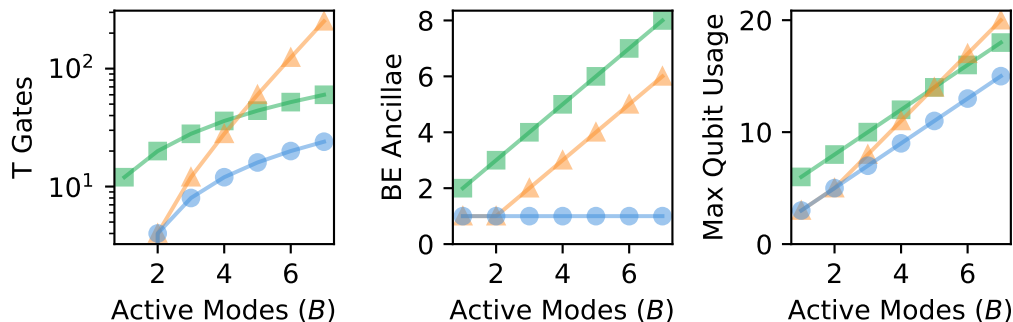


FIG. 13. **Space-time Cost to Block-Encode**  $O = b_0 b_1 \dots b_{B-1} + h.c.$  The number of  $T$  gates (left), block-encoding ancillae (middle), and maximum number of qubits used (right) are shown as a function of the number of active modes ( $B$ ). Results for Pauli Expansion are shown as the orange triangles, results for Piecewise Pauli are shown as the green squares, and results for LOBE are shown as the blue circles. For this operator, all block-encodings use zero non-Clifford rotations. When  $B = 1$  both Pauli Expansion and LOBE require zero  $T$  gates. Both Pauli Expansion and LOBE have rescaling factors of  $\lambda = 1$ , while Piecewise Pauli has a rescaling factor of  $\lambda = 2$ .

( $b_0 b_1 \dots b_{B-1} + h.c.$ ). The numerical space-time costs of the three block-encoding methods for these operators are shown as a function of the number of active modes ( $B$ ) in Figure 13. The associated LOBE constructions for these operators are described in Subsection IV D.

The space-time costs for LOBE and Pauli Expansion are identical for  $B = 1$  and  $B = 2$ . However, the number of required  $T$  gates scales exponentially with  $B$  for Pauli Expansion, yet scales linearly for both Piecewise Pauli and LOBE. Additionally, the LOBE constructions only require a single block-encoding ancilla, independent of  $B$ , while both the Pauli Expansion and Piecewise Pauli methods require a number of block-encoding ancillae that scales linearly with  $B$ .

The second set of block-encodings we consider is those that encode a single bosonic annihilation operator ( $a$ ) with an increasing bosonic occupation cutoff ( $\Omega$ ). Since there is only a single operator, both Pauli methods result in the same construction therefore we refer to these constructions by “Pauli (LCU)”. The numerical space-time costs and rescaling factors of the Pauli (LCU) and LOBE block-encodings are shown in Figure 14. The associated LOBE construction for this operator is described in Subsection IV E.

The LOBE constructions result in block-encodings with fewer required resources for all metrics as compared to the Pauli (LCU) method. Notably, the number of required  $T$  gates scales logarithmically with  $\Omega$  for LOBE, yet scales roughly linearly for the Pauli (LCU) method. Additionally, the number of block-encoding ancillae is constant (1) regardless of  $\Omega$  for LOBE, yet scales logarithmically for the Pauli (LCU) method. Lastly, the LOBE construction results in a rescaling factor that matches the L2 norm, while the Pauli (LCU) construction results in a larger rescaling factor.

The third set of operators we analyze are given as a linear combination of a product of bosonic annihilation

operators acting on different modes plus its Hermitian conjugate: ( $a_0 a_1 \dots a_{B-1} + h.c.$ ). The numerical space-time costs of the various block-encoding constructions for these operators with  $\Omega = 3$  are shown in Figure 15. The associated LOBE constructions for these operators are described in Subsection IV G.

The overall time-complexity scales linearly with  $B$  for the LOBE and Piecewise Pauli constructions, while it scales exponentially for Pauli Expansion. For the space complexity metrics, all methods scale linearly with  $B$ , yet the LOBE constructions have both the smallest prefactor and numerical values. Finally, the LOBE construction results in the lowest rescaling factor of all constructions.

In certain cases - such as when the number of active modes is small or the bosonic occupation cutoff is low - the Pauli Expansion construction can lead to the lowest space-time costs. However, when the number of active modes is large or the bosonic occupation cutoff is high, the LOBE constructions lead to the lowest space-time costs. For all components analyzed here, the Piecewise Pauli constructions have similar asymptotic scalings compared to LOBE, but result in larger numerical space-time costs. For this reason, the Piecewise Pauli construction will be omitted when benchmarking full systems in the following Subsection.

## B. Quartic Harmonic Oscillator

The quartic harmonic oscillator [38, 39, 71] is an extension of the standard harmonic oscillator. In a second-quantized, dimensionless form, the Hamiltonian can be written as:

$$H = a^\dagger a + g (a + a^\dagger)^4 \quad (47)$$

where there is only one bosonic mode.

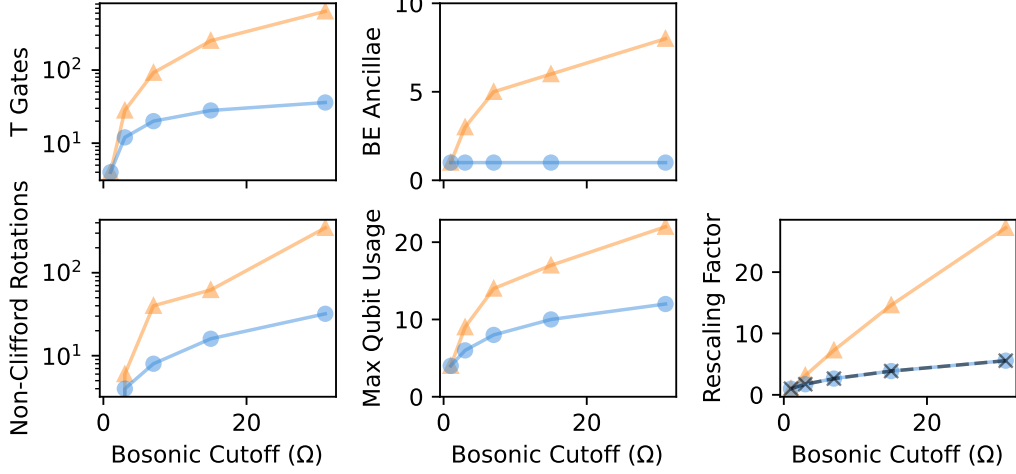


FIG. 14. **Space-time Cost to Block-Encode Bosonic Annihilation Operator** The number of  $T$  gates (upper-left), number of non-Clifford rotations (lower-left), block-encoding ancillae (upper-middle), maximum number of qubits used (lower-middle), and rescaling factor (lower-right) are shown as a function of the bosonic occupation cutoff ( $\Omega$ ). Results for the Pauli (LCU) method are shown as the orange triangles and results for LOBE are shown as the blue circles. The L2 norm of the matrix representing the bosonic annihilation operator with fixed  $\Omega$  is shown as the dashed black crosses.

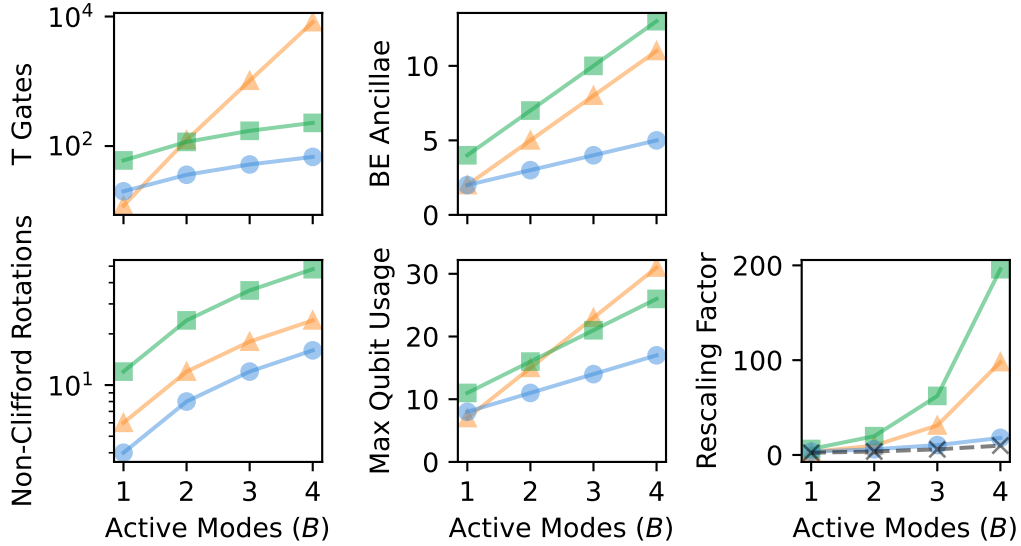


FIG. 15. **Space-time Cost to Block-Encode  $O = a_0 a_1 \dots a_{B-1} + h.c.$**  The number of  $T$  gates (upper-left), number of non-Clifford rotations (lower-left), block-encoding ancillae (upper-middle), maximum number of qubits used (lower-middle), and rescaling factor (lower-right) are shown as a function of the number of active modes ( $B$ ). The bosonic cutoff is fixed to  $\Omega = 3$  for all data points. Results for Pauli Expansion are shown as the orange triangles, results for Piecewise Pauli are shown as the green squares, and results for LOBE are shown as the blue circles. The L2 norm of the matrix representing the operator with  $\Omega = 3$  is shown as the dashed black crosses.

This model is of particular interest as a preliminary test of renormalization of Hamiltonians via Gaussian elimination.

After expanding the product and normal ordering all terms this Hamiltonian can be written as a linear combination of 9 terms consisting of three pairs of operators

plus their Hermitian conjugates, two operators that are their own Hermitian conjugates, and a constant offset:

$$\begin{aligned}
 H = & (12g + 1)a^\dagger a + 6ga^{\dagger 2} a^2 + 6g(a^{\dagger 2} + a^2) \\
 & + 4g(a^{\dagger 3} a + a^\dagger a^3) + g(a^{\dagger 4} + a^4) + 3
 \end{aligned} \tag{48}$$



In Figure 16, we show the scaling of the space-time costs associated with both the LOBE and Pauli Expansion block-encodings as a function of the bosonic occupation cutoff ( $\Omega$ ). For small values of  $\Omega$ , the Pauli Expansion block-encodings result in lower space-time costs, however, the LOBE constructions have favorable scaling and therefore a crossover point is seen.

For the time-complexity, this crossover occurs at  $\Omega = 15$  for the number of  $T$  gates and  $\Omega = 7$  for the number of non-Clifford rotations. For the space-complexity, this crossover occurs at  $\Omega = 7$  for the number of block-encoding ancillae and  $\Omega = 31$  for the maximum number of qubits. Finally, for the rescaling factor, this crossover occurs at  $\Omega = 31$ .

### C. Static Yukawa

The next simplest model that we consider is a non-relativistic approximation to the Yukawa model called the static Yukawa model [72]. This model is taken as the limit of the massive Yukawa model of infinitely heavy fermions, resulting in bosons at rest relative to the fermions that emit/absorb them.

The second-quantized Hamiltonian for the static Yukawa model is given by:

$$H = C_f b^\dagger b + C_b a^\dagger a + g b^\dagger b (a + a^\dagger) \quad (49)$$

where  $C_f$  and  $C_b$  are constants derived from the masses of the free fermion and free boson, respectively, and  $g$  represents the strength of the fermion-boson interaction. In this model, there is one fermionic mode and one bosonic mode so the indices on each mode are omitted. The Renormalization Group Procedure for Effective Particles (RGPEP) [83] is exactly solvable when applied to the static Yukawa model, making this model an interesting system to consider.

As this model is restricted to one fermionic and one bosonic mode, we compare the space-time costs of the different block-encoding methods as a function of the bosonic occupation cutoff ( $\Omega$ ). These numerical results are shown in Figure 17. Similar to the quartic harmonic oscillator, the Pauli Expansion method results in lower space-time costs when the bosonic cutoff is low. However, the LOBE constructions have better asymptotic scaling with respect to  $\Omega$  and crossover points exist for all metrics, above which LOBE results in lower cost constructions.

For the time-complexity, this crossover point occurs at  $\Omega = 3$  for the number of  $T$  gates and the LOBE constructions require fewer non-Clifford rotations at all values of  $\Omega$ . For the space-complexity, this crossover point occurs at  $\Omega = 7$  for the number of block-encoding ancillae and  $\Omega = 15$  for the maximum number of qubits. Finally, for the rescaling factor, this crossover point occurs at  $\Omega = 7$ . At small values of  $\Omega$ , LOBE requires fewer operations but needs more qubits, creating a space-time trade-off. Meanwhile, at larger values of  $\Omega$ , LOBE results in favorable block-encoding constructions for all metrics we consider.

### D. $\phi^4$ Theory

$\phi^4$  theory is one of the simplest interacting field theories. This theory leads to quartic interactions between scalar particles. In lightfront coordinates, the  $\phi^4$  Hamiltonian can be written as:

$$H = \sum_i c_i a_i^\dagger a_i + \sum_{ijkl} c_{ijkl} \left( a_i^\dagger a_j^\dagger a_k^\dagger a_l + h.c. \right) + \sum_{ijkl} \tilde{c}_{ijkl} a_i^\dagger a_j^\dagger a_k a_l \quad (50)$$

where the values of the coefficients are omitted for brevity, but can be determined analytically [73].

Unlike the Quartic Harmonic Oscillator and the Static Massive Yukawa model,  $\phi^4$  theory on the light front is defined based on a discretization of momentum modes. Since the results in Subsections VB and VC establish that LOBE constructions are generally preferred when the bosonic cutoff is large, here we chose to look at the space-time cost as a function of the total number of momentum modes. In Figure 18, we show the scaling of the space-time costs associated with both the LOBE and Pauli Expansion block-encodings as a function of the number of modes. For these estimates, the bosonic cutoff is fixed to  $\Omega = 3$ .

When the number of modes is small (low resolution), the LOBE and Pauli Expansion constructions require similar space-time costs, with the Pauli Expansion block-encodings requiring one fewer block-encoding ancilla when there are only two modes. For higher resolutions (more modes), the LOBE constructions require significantly fewer  $T$  gates and non-Clifford rotations, in

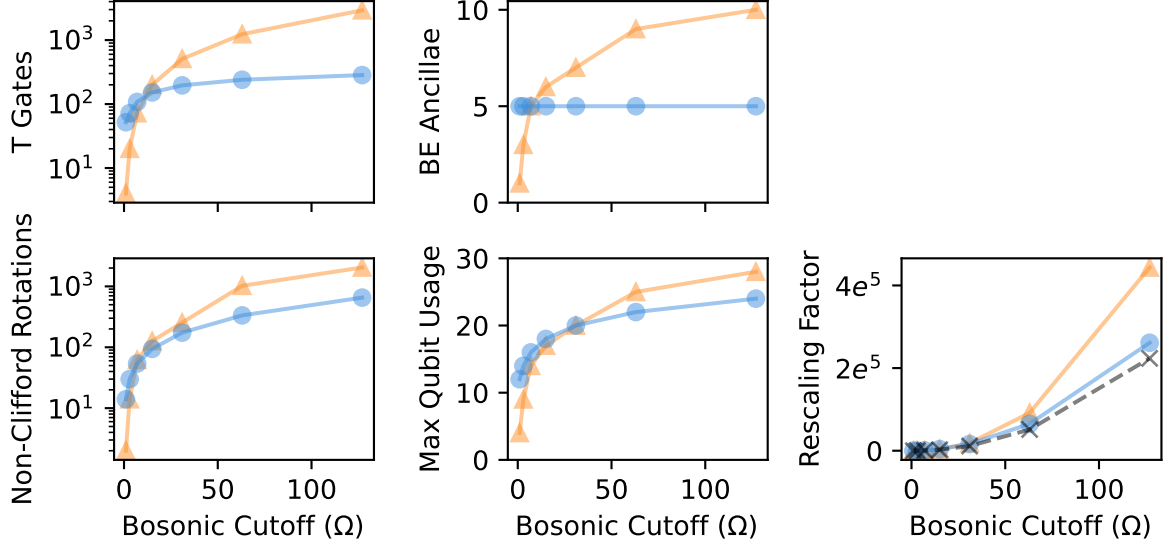


FIG. 16. **Quartic Harmonic Oscillator** The number of  $T$  gates (upper-left), number of non-Clifford rotations (lower-left), block-encoding ancillae (upper-middle), maximum number of qubits used (lower-middle), and rescaling factor (lower-right) are shown as a function of the bosonic occupation cutoff ( $\Omega$ ). The parameter  $g$  is set to 1 for all data points. Results for the Pauli Expansion method are shown as the orange triangles and results for LOBE are shown as the blue circles. The L2 norm of the Hamiltonian is shown as the dashed black crosses.

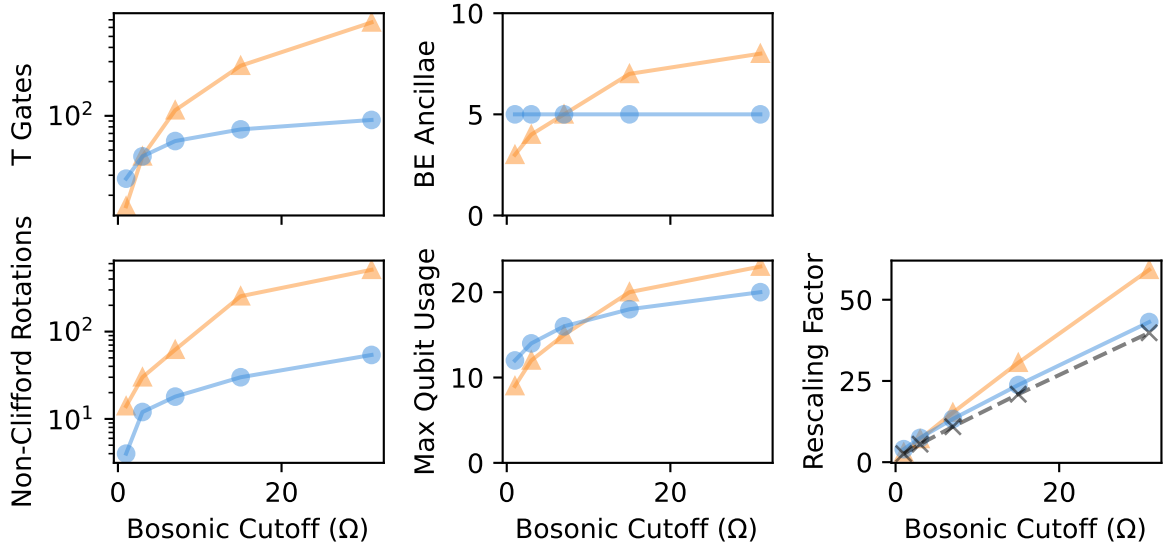


FIG. 17. **Static Massive Yukawa** The number of  $T$  gates (upper-left), number of non-Clifford rotations (lower-left), block-encoding ancillae (upper-middle), maximum number of qubits used (lower-middle), and rescaling factor (lower-right) are shown as a function of the bosonic occupation cutoff ( $\Omega$ ). The parameters  $C_f$ ,  $C_b$ , and  $g$  are set to 1 for all data points. Results for the Pauli Expansion method are shown as the orange triangles and results for LOBE are shown as the blue circles. The L2 norm of the Hamiltonian is shown as the dashed black crosses.

addition to requiring fewer block-encoding ancillae, using fewer total qubits, and having smaller rescaling factors. Notably, when 7 momentum modes are used, the time cost for the LOBE construction is approximately two or-

ders of magnitude smaller than the Pauli Expansion construction.

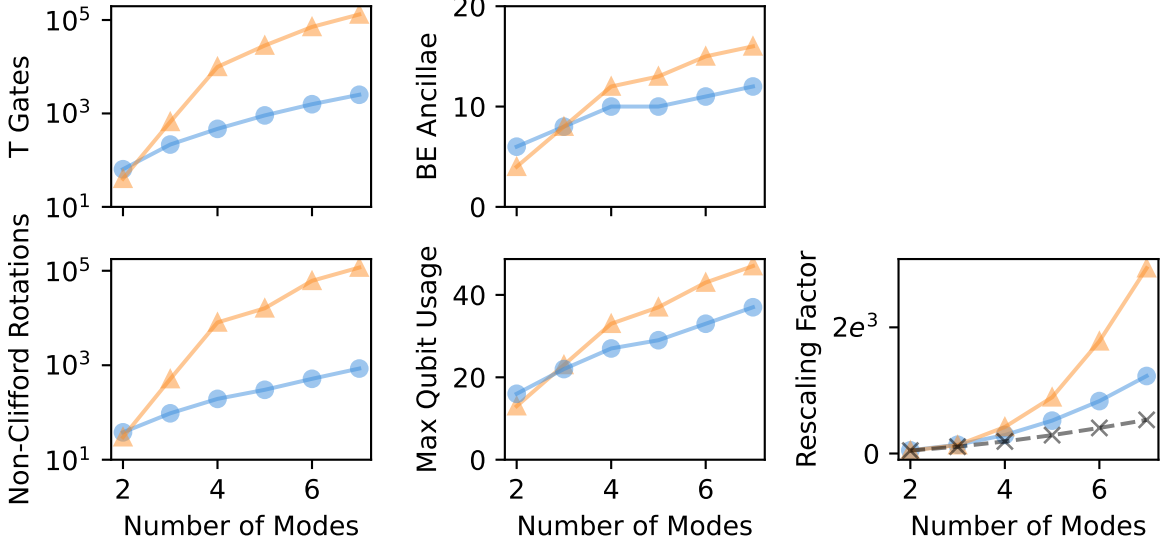


FIG. 18.  $\phi^4$  **Theory** The number of  $T$  gates (upper-left), number of non-Clifford rotations (lower-left), block-encoding ancillae (upper-middle), maximum number of qubits used (lower-middle), and rescaling factor (lower-right) are shown as a function of the number of momentum modes. The bosonic cutoff is fixed to  $\Omega = 3$  and the parameters  $g$  and  $m_b$  are set to 1 for all data points. Results for the Pauli - Expansion method are shown as the orange triangles and results for LOBE are shown as the blue circles. The L2 norm of the Hamiltonian is shown as the dashed black crosses.

### E. Yukawa Theory

In this Subsection, we examine the space-time cost to block-encode the massive Yukawa model, which includes interactions between fermionic, antifermionic, and bosonic modes. This is a theory of interacting fermions and bosons which can be used as a model of the strong nuclear force between hadrons.

The Hamiltonian associated with this Lagrangian can be written in second quantization on the light front as:

$$\begin{aligned}
 H = & \sum_i c_i b_i^\dagger b_i + \sum_i \bar{c}_i d_i^\dagger d_i + \sum_i \tilde{c}_i a_i^\dagger a_i + \\
 & \sum_{ijk} c_{ijk} \left( b_i^\dagger b_j a_k^\dagger + h.c. \right) + \sum_{ijk} \bar{c}_{ijk} \left( d_i^\dagger d_j a_k^\dagger + h.c. \right) + \\
 & \sum_{ijk} \tilde{c}_{ijk} \left( b_i^\dagger d_j^\dagger a_k + h.c. \right) + \sum_{ijkl} c_{ijkl} b_i^\dagger b_j a_k^\dagger a_l + \\
 & \sum_{ijkl} \bar{c}_{ijkl} d_i^\dagger d_j a_k^\dagger a_l + \sum_{ijkl} \tilde{c}_{ijkl} \left( b_i^\dagger d_j^\dagger a_k a_l + h.c. \right)
 \end{aligned} \tag{51}$$

where the values of the coefficients can be determined by classical preprocessing [74].

In Figure 19, the space-time costs for both the Pauli Expansion and LOBE block-encodings are shown as a function of the number of momentum modes. For this model, the LOBE constructions result in fewer required quantum resources for all metrics. Notably, the number of  $T$  gates and number of non-Clifford rotations required

for LOBE is smaller than those required by the Pauli Expansion by a constant factor. Additionally, the bosonic cutoff is set to the smallest nontrivial value ( $\Omega = 3$ ) for the results shown in Figure 19, and the relative improvements from LOBE increase for larger cutoffs.

## VI. CONCLUSIONS

In this work, we detail a framework - which we refer to as LOBE (Ladder Operator Block-Encoding) - that constructs quantum circuits to block-encode operators written directly in second quantization. We give explicit compilations for operators written as linear combinations of products of ladder operators acting on both fermionic and bosonic modes and detail how these constructions can be generalized to other types of operators. This avoids expanding operators in the Pauli basis prior to block-encoding which introduces a significant overhead. Additionally, we provide an open-source library to build these block-encoding circuits for various second-quantized operators [75].

We provide analytical and numerical spacetime costs for the relevant quantum resources required by LOBE. We compare our constructions to those that require expressing the operators in the Pauli basis using the Jordan-Wigner and Standard Binary transformations. Our numerical results show that in most relevant cases, the LOBE framework produces block-encodings that require significantly fewer  $T$  gates, non-Clifford rotations, block-encoding ancillae and total number of qubits and

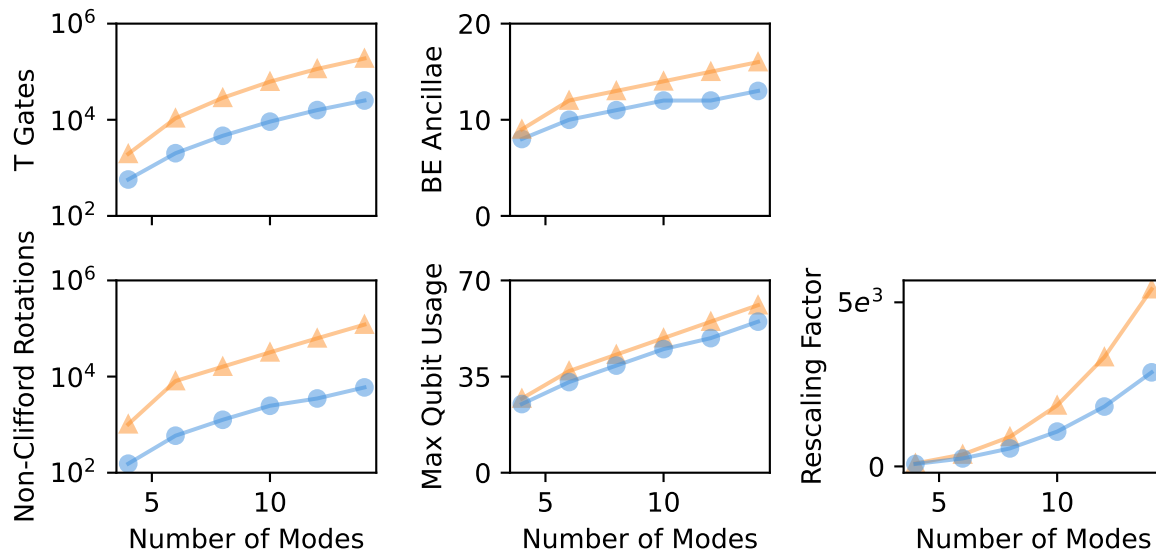


FIG. 19. **Massive Yukawa** The number of  $T$  gates (upper-left), number of non-Clifford rotations (lower-left), block-encoding ancillae (upper-middle), maximum number of qubits used (lower-middle), and rescaling factor (lower-right) are shown as a function of the number of momentum modes. The bosonic cutoff is fixed to  $\Omega = 3$  and the parameters  $m_f$ ,  $m_b$ , and  $g$  are set to 1 for all data points. Results for the Pauli - Expansion method are shown as the orange triangles and results for LOBE are shown as the blue circles.

result in block-encodings with smaller rescaling factors. In addition, the LOBE framework has favorable scaling with respect to the maximum occupation of bosonic modes, the number of momentum modes, and the locality of the operator.

In certain cases, such as when block-encoding a product of fermionic operators with its Hermitian conjugate, LOBE results in exponentially fewer non-Clifford operations with respect to the locality as compared to a naive expansion of the operator in the Pauli basis. However, when considering a linear combination of such operators with the same active modes, the Pauli transformation can lead to cancellations which make expanding in the Pauli basis favorable. A more thorough comparison between these frameworks for operators with this form, such as those arising in quantum chemistry, is needed and we leave this for future work.

The framework presented in this work allows for the construction of block-encodings for operators acting on fermionic, antifermionic, and bosonic modes written directly in their second-quantized form. Many operators arising in both quantum chemistry and quantum field theories are expressed efficiently in second quantization, making this framework particularly well-suited for these

operators. By reducing the quantum resources required to block-encode these operators, this work paves the way for compiling efficient quantum algorithms that simulate quantum systems.

## VII. ACKNOWLEDGEMENTS

We thank William Kirby, Michael Kreshchuk, James Vary, Pieter Maris, Chao Yang and Weijie Du for productive discussions. William A. Simon is supported by the Department of Defense (DoD) through the National Defense Science & Engineering Graduate (NDSEG) Fellowship Program. Carter Gustin was supported by the **EXCLUSIVES** via **Artificial Intelligence and Machine Learning (EXCLAIM)** collaboration, DOE grant DE-SC0024644. Kamil Serafin, Peter Love and Gary Goldstein were supported by US DOE Grant DE-SC0023707 under the Office of Nuclear Physics Quantum Horizons program for the “**Nuclei and Hadrons with Quantum computers (NuHaQ)**” project. Alexis Ralli was supported by the STAQ project under award NSF-PHY-232580. This material is based upon work supported by the U.S. Department of Energy (DOE), Office of Science, National Quantum Information Science Research Centers, Quantum Systems Accelerator.

[1] R. P. Feynman, Simulating physics with computers, in *Feynman and computation* (cRc Press, 2018) pp. 133–153.

[2] S. Lloyd, Universal quantum simulators, *Science* **273**, 1073 (1996).

- [3] D. A. Meyer, From quantum cellular automata to quantum lattice gases, *Journal of Statistical Physics* **85**, 551 (1996).
- [4] B. M. Boghosian and W. Taylor, Quantum lattice-gas models for the many-body schrödinger equation, *International Journal of Modern Physics C* **8**, 705 (1997).
- [5] D. S. Abrams and S. Lloyd, Quantum algorithm providing exponential speed increase for finding eigenvalues and eigenvectors, *Physical Review Letters* **83**, 5162 (1999).
- [6] D. A. Lidar and H. Wang, Calculating the thermal rate constant with exponential speedup on a quantum computer, *Physical Review E* **59**, 2429 (1999).
- [7] B. M. Terhal and D. P. DiVincenzo, Problem of equilibration and the computation of correlation functions on a quantum computer, *Physical Review A* **61**, 022301 (2000).
- [8] L.-A. Wu, M. Byrd, and D. Lidar, Polynomial-time simulation of pairing models on a quantum computer, *Physical Review Letters* **89**, 057904 (2002).
- [9] A. Aspuru-Guzik, A. D. Dutoi, P. J. Love, and M. Head-Gordon, Simulated quantum computation of molecular energies, *Science* **309**, 1704 (2005).
- [10] I. Kassal, S. P. Jordan, P. J. Love, M. Mohseni, and A. Aspuru-Guzik, Polynomial-time quantum algorithm for the simulation of chemical dynamics, *Proceedings of the National Academy of Sciences* **105**, 18681 (2008).
- [11] U.-J. Wiese, Towards quantum simulating qcd, *Nuclear Physics A* **931**, 246 (2014).
- [12] S. P. Jordan, K. S. Lee, and J. Preskill, Quantum algorithms for quantum field theories, *Science* **336**, 1130 (2012).
- [13] Y. Cao, J. Romero, J. P. Olson, M. Degroote, P. D. Johnson, M. Kieferová, I. D. Kivlichan, T. Menke, B. Peropadre, N. P. Sawaya, *et al.*, Quantum chemistry in the age of quantum computing, *Chemical reviews* **119**, 10856 (2019).
- [14] S. McArdle, S. Endo, A. Aspuru-Guzik, S. C. Benjamin, and X. Yuan, Quantum computational chemistry, *Reviews of Modern Physics* **92**, 015003 (2020).
- [15] C. W. Bauer, Z. Davoudi, A. B. Balantekin, T. Bhattacharya, M. Carena, W. A. De Jong, P. Draper, A. El-Khadra, N. Gemelke, M. Hanada, *et al.*, Quantum simulation for high-energy physics, *PRX quantum* **4**, 027001 (2023).
- [16] M. Suzuki, Generalized trotter's formula and systematic approximants of exponential operators and inner derivations with applications to many-body problems, *Communications in Mathematical Physics* **51**, 183 (1976).
- [17] N. Hatano and M. Suzuki, Finding exponential product formulas of higher orders, in *Quantum annealing and other optimization methods* (Springer, 2005) pp. 37–68.
- [18] S. Lie, *Theorie der Transformationsgruppen*, Vol. 3 (Teubner, 1893).
- [19] H. F. Trotter, On the product of semi-groups of operators, *Proceedings of the American Mathematical Society* **10**, 545 (1959).
- [20] A. M. Childs, Y. Su, M. C. Tran, N. Wiebe, and S. Zhu, Theory of trotter error with commutator scaling, *Physical Review X* **11**, 011020 (2021).
- [21] L. Lin, Lecture notes on quantum algorithms for scientific computation, arXiv preprint arXiv:2201.08309 (2022).
- [22] D. Poulin, A. Kitaev, D. S. Steiger, M. B. Hastings, and M. Troyer, Quantum algorithm for spectral measurement with a lower gate count, *Physical review letters* **121**, 010501 (2018).
- [23] G. H. Low and I. L. Chuang, Hamiltonian simulation by qubitization, *Quantum* **3**, 163 (2019).
- [24] D. W. Berry and A. M. Childs, Black-box hamiltonian simulation and unitary implementation, *Quantum Information & Computation* **12**, 29 (2012).
- [25] A. M. Childs, Universal computation by quantum walk, *Physical review letters* **102**, 180501 (2009).
- [26] A. M. Childs and N. Wiebe, Hamiltonian simulation using linear combinations of unitary operations, *Quantum Information & Computation* **12**, 901 (2012).
- [27] R. Babbush, C. Gidney, D. W. Berry, N. Wiebe, J. McClean, A. Paler, A. Fowler, and H. Neven, Encoding electronic spectra in quantum circuits with linear t complexity, *Physical Review X* **8**, 041015 (2018).
- [28] D. Bluvstein, S. J. Evered, A. A. Geim, S. H. Li, H. Zhou, T. Manovitz, S. Ebadi, M. Cain, M. Kalinowski, D. Hangleiter, *et al.*, Logical quantum processor based on reconfigurable atom arrays, *Nature* **626**, 58 (2024).
- [29] Google Quantum AI and Collaborators, Quantum error correction below the surface code threshold, *Nature* **638**, 920 (2025).
- [30] A. Peruzzo, J. McClean, P. Shadbolt, M.-H. Yung, X.-Q. Zhou, P. J. Love, A. Aspuru-Guzik, and J. L. O'Brien, A variational eigenvalue solver on a photonic quantum processor, *Nature communications* **5**, 4213 (2014).
- [31] R. Babbush, P. J. Love, and A. Aspuru-Guzik, Adiabatic quantum simulation of quantum chemistry, *Scientific reports* **4**, 6603 (2014).
- [32] P. J. O'Malley, R. Babbush, I. D. Kivlichan, J. Romero, J. R. McClean, R. Barends, J. Kelly, P. Roushan, A. Tranter, N. Ding, *et al.*, Scalable quantum simulation of molecular energies, *Physical Review X* **6**, 031007 (2016).
- [33] G. A. Quantum, Collaborators\*†, F. Arute, K. Arya, R. Babbush, D. Bacon, J. C. Bardin, R. Barends, S. Boixo, M. Broughton, B. B. Buckley, *et al.*, Hartree-fock on a superconducting qubit quantum computer, *Science* **369**, 1084 (2020).
- [34] J. Lee, D. W. Berry, C. Gidney, W. J. Huggins, J. R. McClean, N. Wiebe, and R. Babbush, Even more efficient quantum computations of chemistry through tensor hypercontraction, *PRX Quantum* **2**, 030305 (2021).
- [35] I. D. Kivlichan, C. Gidney, D. W. Berry, N. Wiebe, J. McClean, W. Sun, Z. Jiang, N. Rubin, A. Fowler, A. Aspuru-Guzik, *et al.*, Improved fault-tolerant quantum simulation of condensed-phase correlated electrons via trotterization, *Quantum* **4**, 296 (2020).
- [36] E. T. Campbell, Early fault-tolerant simulations of the hubbard model, *Quantum Science and Technology* **7**, 015007 (2021).
- [37] M. E. Peskin and D. V. Schroeder, *An Introduction to quantum field theory* (Addison-Wesley, Reading, USA, 1995).
- [38] M. Girguś and S. D. Glazek, Spiral flow of quantum quartic oscillator with energy cutoff (2024), arXiv:2404.17446 [quant-ph].
- [39] C. M. Bender and T. T. Wu, Anharmonic oscillator, *Phys. Rev.* **184**, 1231 (1969).
- [40] W. M. Kirby, S. Hadi, M. Kreshchuk, and P. J. Love, Quantum simulation of second-quantized hamiltonians in compact encoding, *Physical Review A* **104**, 10.1103/physreva.104.042607 (2021).

- [41] D. Camps, L. Lin, R. Van Beeumen, and C. Yang, Explicit quantum circuits for block encodings of certain sparse matrices, *SIAM Journal on Matrix Analysis and Applications* **45**, 801 (2024).
- [42] D. Liu, W. Du, L. Lin, J. P. Vary, and C. Yang, An efficient quantum circuit for block encoding a pairing hamiltonian, *Journal of Computational Science* **85**, 102480 (2025).
- [43] M. L. Rhodes, M. Kreshchuk, and S. Pathak, Exponential improvements in the simulation of lattice gauge theories using near-optimal techniques, *PRX Quantum* **5**, 040347 (2024).
- [44] S. Hariprakash, N. S. Modi, M. Kreshchuk, C. F. Kane, and C. W. Bauer, Strategies for simulating the time evolution of hamiltonian lattice field theories, *Physical Review A* **111**, 022419 (2025).
- [45] W. Du and J. P. Vary, Systematic input scheme for many-boson hamiltonians with applications to the two-dimensional  $\phi^4$  theory, *Physical Review D* **111**, 016013 (2025).
- [46] P. Jordan and E. Wigner, Über das paulische Äquivalenzverbot, *Zeitschrift für Physik* **47** (1928).
- [47] S. B. Bravyi and A. Y. Kitaev, Fermionic quantum computation, *Annals of Physics* **298**, 210 (2002).
- [48] J. T. Seeley, M. J. Richard, and P. J. Love, The bravyi-kitaev transformation for quantum computation of electronic structure, *The Journal of chemical physics* **137** (2012).
- [49] R. D. Somma, Quantum computation, complexity, and many-body physics, Ph. D. Thesis (2005).
- [50] N. P. D. Sawaya, T. Menke, T. H. Kyaw, S. Johri, A. Aspuru-Guzik, and G. G. Guerreschi, Resource-efficient digital quantum simulation of d-level systems for photonic, vibrational, and spin-s hamiltonians, *npj Quantum Information* **6**, 49 (2020).
- [51] F. Berezin, *The Method of Second Quantization*, Pure and applied physics : a series of monographs and textbooks. 24 (Academic Press, 1966).
- [52] M. D. Schwartz, *Quantum Field Theory and the Standard Model* (Cambridge University Press, 2013).
- [53] W. Pauli, Über den zusammenhang des abschlusses der elektronengruppen im atom mit der komplexstruktur der spektren, *Zeitschrift für Physik* **31**, 765 (1925).
- [54] M. Kreshchuk, W. M. Kirby, G. Goldstein, H. Beauchemin, and P. J. Love, Quantum simulation of quantum field theory in the light-front formulation, *Physical Review A* **105**, 032418 (2022).
- [55] S. Chakraborty, A. Gilyén, and S. Jeffery, The power of block-encoded matrix powers: Improved regression techniques via faster hamiltonian simulation, in *46th International Colloquium on Automata, Languages, and Programming (ICALP 2019)* (Schloss Dagstuhl–Leibniz-Zentrum für Informatik, 2019) pp. 33–1.
- [56] D. W. Berry, A. M. Childs, and R. Kothari, Hamiltonian simulation with nearly optimal dependence on all parameters, in *2015 IEEE 56th annual symposium on foundations of computer science* (IEEE, 2015) pp. 792–809.
- [57] D. W. Berry, A. M. Childs, R. Cleve, R. Kothari, and R. D. Somma, Simulating hamiltonian dynamics with a truncated taylor series, *Physical review letters* **114**, 090502 (2015).
- [58] G. H. Low and I. L. Chuang, Optimal hamiltonian simulation by quantum signal processing, *Physical review letters* **118**, 010501 (2017).
- [59] A. M. Childs, R. Kothari, and R. D. Somma, Quantum algorithm for systems of linear equations with exponentially improved dependence on precision, *SIAM Journal on Computing* **46**, 1920 (2017).
- [60] A. Gilyén, Y. Su, G. H. Low, and N. Wiebe, Quantum singular value transformation and beyond: exponential improvements for quantum matrix arithmetics, in *Proceedings of the 51st Annual ACM SIGACT Symposium on Theory of Computing* (2019) pp. 193–204.
- [61] D. Camps and R. Van Beeumen, Fable: Fast approximate quantum circuits for block-encodings, in *2022 IEEE International Conference on Quantum Computing and Engineering (QCE)* (IEEE, 2022) pp. 104–113.
- [62] C. Sanavio, E. Mauri, and S. Succi, Explicit quantum circuit for simulating the advection-diffusion-reaction dynamics, *IEEE Transactions on Quantum Engineering* (2025).
- [63] L. Grover and T. Rudolph, Creating superpositions that correspond to efficiently integrable probability distributions, arXiv preprint quant-ph/0208112 (2002).
- [64] D. Jennings, M. Lostaglio, S. Pallister, A. T. Sornborger, and Y. Subaşı, Efficient quantum linear solver algorithm with detailed running costs, arXiv preprint arXiv:2305.11352 (2023).
- [65] P. Selinger, Quantum circuits of t-depth one, *Physical Review A—Atomic, Molecular, and Optical Physics* **87**, 042302 (2013).
- [66] C. Jones, Low-overhead constructions for the fault-tolerant toffoli gate, *Physical Review A—Atomic, Molecular, and Optical Physics* **87**, 022328 (2013).
- [67] A. Barenco, C. H. Bennett, R. Cleve, D. P. DiVincenzo, N. Margolus, P. Shor, T. Sleator, J. A. Smolin, and H. Weinfurter, Elementary gates for quantum computation, *Physical review A* **52**, 3457 (1995).
- [68] C. Gidney, Constructing large increment gates (2015).
- [69] M. Möttönen, J. J. Vartiainen, V. Bergholm, and M. M. Salomaa, Transformation of quantum states using uniformly controlled rotations, *Quantum Information & Computation* **5**, 467 (2005).
- [70] C. Gidney, Halving the cost of quantum addition, *Quantum* **2**, 74 (2018).
- [71] K. P. Wójcik, Application of a numerical renormalization group procedure to an elementary anharmonic oscillator (2012), arXiv:1210.1703 [quant-ph].
- [72] S. D. Glazek, Elementary example of exact effective-hamiltonian computation, *Phys. Rev. D* **103**, 014021 (2021).
- [73] J. P. Vary, M. Huang, S. Jawadekar, M. Sharaf, A. Harindranath, and D. Chakrabarti, Critical coupling for two-dimensional  $\phi^4$  theory in discretized light-cone quantization, *Phys. Rev. D* **105**, 016020 (2022).
- [74] H.-C. Pauli and S. J. Brodsky, Solving field theory in one space and one time dimension, *Phys. Rev. D* **32**, 1993 (1985).
- [75] W. A. Simon, C. Gustin, K. Serafin, and A. Ralli, LOBE, <https://github.com/Tufts-QIQC/LOBE> (2024).
- [76] C. Gustin, W. A. Simon, E. Guo, K. Serafin, and A. Ralli, OpenParticle, <https://github.com/cgustin99/OpenParticle> (2024).
- [77] T. Weaving, A. Ralli, P. J. Love, S. Succi, and P. V. Coveney, Contextual subspace variational quantum eigensolver calculation of the dissociation curve of molecular nitrogen on a superconducting quantum computer, *npj Quantum Information* **11**, 10.1038/s41534-

- 024-00952-4 (2025).
- [78] A. Ralli, T. Weaving, A. Tranter, W. M. Kirby, P. J. Love, and P. V. Coveney, Unitary partitioning and the contextual subspace variational quantum eigensolver, *Phys. Rev. Res.* **5**, 013095 (2023).
- [79] T. Weaving, A. Ralli, W. M. Kirby, A. Tranter, P. J. Love, and P. V. Coveney, A stabilizer framework for the contextual subspace variational quantum eigensolver and the noncontextual projection ansatz, *Journal of Chemical Theory and Computation* **19**, 808 (2023), pMID: 36689668, <https://doi.org/10.1021/acs.jctc.2c00910>.
- [80] W. M. Kirby, A. Tranter, and P. J. Love, Contextual Subspace Variational Quantum Eigensolver, *Quantum* **5**, 456 (2021).
- [81] Q. A. team and collaborators, *Cirq* (2020).
- [82] grover-rudolph (2024).
- [83] S. D. Glazek, Perturbative formulae for relativistic interactions of effective particles, *Acta Phys. Polon. B* **43**, 1843 (2012), arXiv:1204.4760 [hep-th].
- [84] M. A. Nielsen and I. L. Chuang, *Quantum computation and quantum information*, Vol. 2 (Cambridge university press Cambridge, 2001).
- [85] A. Y. Kitaev, Quantum measurements and the abelian stabilizer problem, arXiv preprint quant-ph/9511026 (1995).
- [86] P. A. M. Dirac, Forms of relativistic dynamics, *Rev. Mod. Phys.* **21**, 392 (1949).

### Appendix A: Glossary

In this Section, we explicitly define some of the technical phrases and symbols used throughout this work.

- *Active Mode*: A fermionic or bosonic mode upon which a ladder operator is being non-trivially applied.
- *block-encoding ancillae*: A register of qubits that give additional degrees of freedom to produce a block-encoding for the operator in a larger Hilbert space.
- *encoded subspace*: The chosen subspace of the block-encoding ancillae that denotes the subspace in which the non-unitary operator is encoded. Typically, this is the subspace where all block-encoding ancillae are in the  $|0\rangle$  state.
- *clean ancillae*: A register of qubits that are promised to begin in the  $|0\rangle$  and are returned to the  $|0\rangle$  state at the end of a particular operation.
- *all-zero state*: A state of a register where all qubits are in the  $|0\rangle$  state.
- $L$ : The number of terms in the Hamiltonian.
- $\alpha_l$ : The coefficient of the  $l^{\text{th}}$  term in a linear combination. Assumed to be real and positive unless otherwise stated.
- $O_l$ : The  $l^{\text{th}}$  operator in a linear combination.
- $\Omega$ : The occupation cutoff for the bosonic modes.  $\Omega$  gives the maximum number of bosons that can be present in a single mode.
- $I$ : The number of fermionic or bosonic modes. The subscripts  $b$  and  $a$  will be used to denote the number of fermionic and bosonic modes respectively.
- $b_i$ : Fermionic annihilation (creation -  $b_i^\dagger$ ) operator acting on mode  $i$ .
- $d_i$ : Antifermionic annihilation (creation -  $d_i^\dagger$ ) operator acting on mode  $i$ .
- $a_i$ : Bosonic annihilation (creation -  $a_i^\dagger$ ) operator acting on mode  $i$ .
- $n_i$ : The number of fermions occupying the  $i^{\text{th}}$  mode.
- $\omega_i$ : The number of bosons occupying the  $i^{\text{th}}$  bosonic mode.
- $N_A$ : The dimension of a matrix  $A$ .
- $U_A$ : A unitary matrix providing a block-encoding of the matrix  $A$ .
- $\beta_\psi$ : The amplitude of a state that is outside of the encoded subspace after a block-encoding unitary is applied to  $|\psi\rangle$ .
- $\lambda$ : The rescaling factor imposed on the operator for a given block-encoding.
- $s$ : The sparsity of a matrix.
- $\mathcal{S}$ : An integer power-of-two for the sparsity of a matrix, obtained by treated zero-valued entries as nonzero.  $\mathcal{S} = 2^{\lceil \log_2 s \rceil}$
- $W$ : The number of qubits storing the occupation state of bosonic modes.  $W = \lceil \log_2 \Omega \rceil$ .
- $w$ : The index of the  $w^{\text{th}}$  least-significant bit in a binary encoding.
- $B$ : The number of active modes within an operator.
- $C$ : The number of active modes within an operator *excluding* modes upon which a number operator is being applied.
- $S_{l,i}$ : The exponent of bosonic annihilation operators acting on the  $i^{\text{th}}$  bosonic mode within the  $l^{\text{th}}$  term.
- $R_{l,i}$ : The exponent of bosonic creation operators acting on the  $i^{\text{th}}$  bosonic mode within the  $l^{\text{th}}$  term.
- $P$ : The sum of the exponents of bosonic ladder operators acting on all modes within a single term.

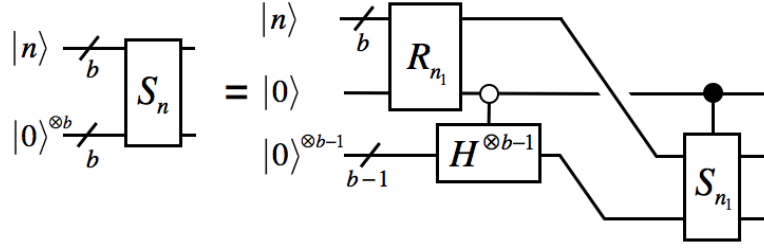


FIG. 20. The quantum circuits showing the recursive definition of the algorithm to prepare a uniform superposition of the first  $n$  logical basis states. Here  $n_1 = n - 2^{\lceil \log_2 n \rceil}$ ,  $R_{n_1}$  is the rotation defined in equation B7 where  $n$  is a parameter for the rotation, and  $H$  is the Hadamard gate. This recursive procedure is applied until  $n_1$  is a power of two.

## Appendix B: Uniform State Preparation

In the interests of keeping the paper self-contained, in this section we present an algorithm for the preparation of the uniform superposition of  $n$  logical basis states  $|l\rangle$  for  $0 \leq l \leq n - 1$ . That is, we obtain a quantum circuit for the operator  $S_n$ :

$$S_n |0\rangle^{\otimes b} = \frac{1}{\sqrt{n}} \sum_{l=0}^{n-1} |l\rangle. \quad (\text{B1})$$

If  $n = 2^b$  it is well known that this can be accomplished by the application of  $b$  Hadamard gates [84]:

$$\frac{1}{\sqrt{2^b}} \sum_{l=0}^{2^b-1} |l\rangle = (H |0\rangle)^{\otimes b}. \quad (\text{B2})$$

The superposition for  $n \neq 2^b$  can also be prepared efficiently by the method of [85]. First, we take  $b = \lceil \log_2 n \rceil$ .

So that we may write:

$$S_n = \left[ \Lambda_0(H^{\otimes b-1}) + \Lambda_1(S_{n_1}) \right] \left[ R_n \otimes 1^{\otimes b-1} \right] \quad (\text{B6})$$

where the single qubit rotation  $R_n$  is defined by:

$$R_n = \frac{1}{\sqrt{n}} \begin{pmatrix} \sqrt{2^{b-1}} & \sqrt{n_1} \\ \sqrt{n_1} & \sqrt{2^{b-1}} \end{pmatrix} \quad (\text{B7})$$

This procedure, which is represented by the circuit in Figure 20, is repeated until  $n_1$  is a power of two, in which case the method of eq. B2 is used. The cost of this procedure is maximal when  $n = 2^a - 1$ , in which case at each stage of the recursion  $n_1$  is also of the form  $2^{a'} - 1$ , and asymptotically the cost scales as  $\mathcal{O}(b^2)$ . In addition to this, if  $n$  is provided in a second register, there will be an additional ancilla cost due to the need to coherently

Write  $n = 2^{b-1} + n_1$  and proceed recursively:

$$\frac{1}{\sqrt{n}} \sum_{l=0}^{n-1} |l\rangle = \frac{1}{\sqrt{n}} \sum_{l=0}^{2^{b-1}-1} |l\rangle + \frac{1}{\sqrt{n}} \sum_{l=2^{b-1}}^{n-1} |l\rangle \quad (\text{B3})$$

the highest of the  $b$  bits is always zero in the first sum, and always one in the second sum. Hence we may write:

$$\frac{1}{\sqrt{n}} \sum_{l=0}^{n-1} |l\rangle = \sqrt{\frac{2^{b-1}}{n}} |0\rangle \frac{1}{\sqrt{2^{b-1}}} \sum_{l=0}^{2^{b-1}-1} |l\rangle + \sqrt{\frac{n_1}{n}} |1\rangle \frac{1}{\sqrt{n_1}} \sum_{l=0}^{n_1-1} |l\rangle. \quad (\text{B4})$$

This gives a recursive procedure for the definition of  $S_n$  in terms of  $S_{n_1}$ :

$$\begin{aligned} S_n |0\rangle^{\otimes b} &= \sqrt{\frac{2^{b-1}}{n}} |0\rangle (H |0\rangle)^{\otimes b-1} + \sqrt{\frac{n_1}{n}} |1\rangle S_{n_1} |0\rangle^{\otimes b-1} \\ &= [\Lambda_0(H^{\otimes b-1}) + \Lambda_1(S_{n_1})] \left[ \sqrt{\frac{2^{b-1}}{n}} |0\rangle + \sqrt{\frac{n_1}{n}} |1\rangle \right] |0\rangle^{\otimes b-1} \end{aligned} \quad (\text{B5})$$

compute the angles of the rotations  $R_{n_1}$  so that they can be applied by phase kickback.

## Appendix C: Compiling Toffoli Gates

The Toffoli gate is a ubiquitous operation in quantum algorithms and is often a significant contributor to the number of non-Clifford resources. In many algorithms - including those described in this work - a series of Toffoli gates are used to perform an operation that is coherently controlled on the logical-AND of several variables (Figure 22). Therefore, even small reductions in the cost of compiling a Toffoli gate can have a significant impact on the overall space-time cost of an algorithm. In an effort to keep this work self-contained, we review a specific compilation technique that can reduce the number of  $T$



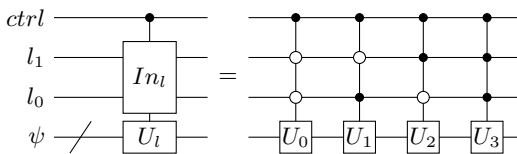


FIG. 21. **Uniformly Controlled Operations** A series of operations that are subsequently controlled on the computational basis states of a register are referred to as *uniformly controlled operations*.

gates required to synthesize a pair of  $N$ -controlled Toffoli gates.

In Nielsen and Chuang [84], a method for synthesizing a single Toffoli gate from 7  $T$  gates is shown which is likely derived from the methods proposed by Barenco et al. [67]. Selinger [65] and Jones [66] reduce this cost for a single Toffoli gate from 7  $T$  gates to 4 using one clean ancilla. To the best of our knowledge, this is the most  $T$ -gate efficient compilation for a single Toffoli gate.

Gidney [70] showed that a pair of Toffoli gates which subsequently compute and uncompute the logical-AND of two variables can be synthesized using 4  $T$  gates, a measurement, and a classically conditioned operation (Figure 3 of [70]). This compilation scheme is sometimes referred to as “elbows” and is depicted in Figure 23.

Following the methods shown by Barenco et al. [67] and Gidney [70], a pair of  $N$ -controlled Toffoli gates that are used to compute and uncompute the logical-AND of the same variables can be composed using  $4(N - 1)$   $T$  gates and  $N - 1$  clean ancilla using a series of elbows. It is important to note that this technique does not always apply to neighboring Toffoli gates, but sufficient conditions are given in Figure 5 of [70]. The space-time costs for the block-encoding circuits used in this work assume this strategy when applicable.

Additionally, there are several optimizations that can reduce the cost of neighboring pairs of elbows which are shown in Figure 6 of Babbush et al. [27]. These optimizations are particularly useful when compiling uniformly controlled operations (Figure 21). With these optimizations, the control structure for applying  $L$  uniformly controlled operations uses  $4(L - 1)$   $T$  gates. The space-time costs quoted throughout this work assume this strategy when applicable, including in cases such as Figures 11 and 12.

#### Appendix D: Addition by a Known Classical Value

Adding a (known) classical integer ( $m$ ) to a quantum register encoded in binary is a required operation throughout this work:

$$|n\rangle \rightarrow |n + m\rangle \quad (\text{D1})$$

In an effort to keep this work self-contained and pedagogical, we review some methods for constructing this

operation in this Section.

One option is to use a series of controlled incrementer ( $+1$ ) circuits. An implementation of an incrementer circuit given by Gidney [68] is shown in Figure 24. If  $N$  is the number of qubits in the register being incremented, this implementation requires  $4(N - 1)$   $T$  gates and  $N - 1$  clean ancillae. Naively, a series of  $m$  incrementers will result in increasing the value of the register by  $m \bmod 2^N$ .

However, an incrementer circuit can also be used to perform addition by a power of 2 by acting on only the most-significant qubits. For example, adding the value 8 can be achieved using an incrementer circuit that treats the 4<sup>th</sup> least significant qubit as the least significant qubit in the incrementer circuit and disregards the 3 lesser qubits. A circuit adding any classical value can then be constructed based on the binary representation of the classical number. A circuit diagram for this construction is shown in Figure 25. The cost of this construction would require  $N$  incrementer circuits requiring  $4 \sum_{i=0}^{N-2} N - i - 1$   $T$  gates in total and  $N - 1$  clean ancillae.

Since we are performing modular addition, the same result can also be achieved by subtracting the value  $2^N - m$ . As an example, if the classical value is 31 and  $N = 5$ , then this can be accomplished using a single decremter circuit which can be constructed by conjugating an incrementer circuit with Pauli X gates acting on the qubits encoding  $|n\rangle$ . The cost of these two methods can be classically determined and the more favorable option can be chosen during compilation.

Another option is to first load the classical value into a clean ancilla register, controlled on the control qubit, perform *uncontrolled* (modular) addition of the two quantum registers, then “unload” the classical value. If the control is off, then the classical value is not loaded and the uncontrolled addition simply adds the value 0 and leaves the original register unchanged. An example diagram for this construction depicting adding the value  $m = 11$  to a register with  $N = 5$  qubits is shown in Figure 26.

The loading (and unloading) of the classical value only requires CNOTs and therefore does not contribute any non-Clifford resources, but it does require  $N$  clean ancillae. However, if the  $p$  least significant bits of  $m$  are zero, then only  $N - p$  qubits are required to load  $m$  and the  $p$  least-significant qubits of  $N$  can be omitted from the addition. Uncontrolled addition of two registers can be performed using  $4(N - 1)$   $T$  gates and  $N - 1$  clean ancillae using the construction for addition shown in Figure 1 of [70]. Therefore, in total, this compilation will require  $4(N - p - 1)$   $T$  gates and  $2(N - p) - 1$  clean ancillae.

When  $m$  is a power of 2, then compilation using incrementer circuits uses the same number of  $T$  gates, but fewer clean ancillae. When  $m$  is not a power of 2, then the compilation using uncontrolled quantum addition uses fewer  $T$  gates (at the expense of more clean ancillae). Since  $m$  is known during compilation, an implementation can be chosen that results in the fewest required resources.

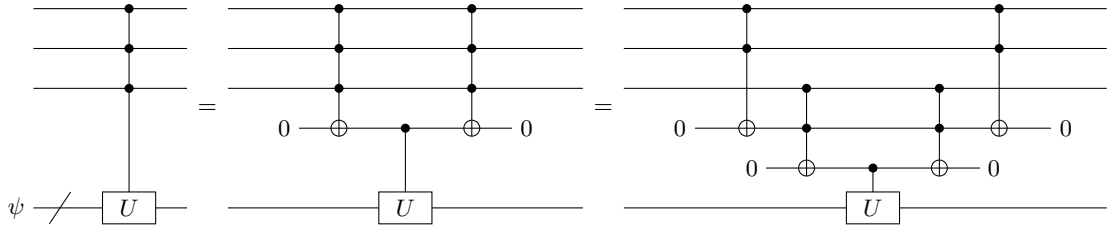


FIG. 22. **Multi-Controlled Operations** Operations with multiple controls are referred to as *multi-controlled operations*. An  $N$ -controlled operation can be decomposed into  $2(N - 1)$  Toffoli gates using  $N - 1$  clean ancillae.

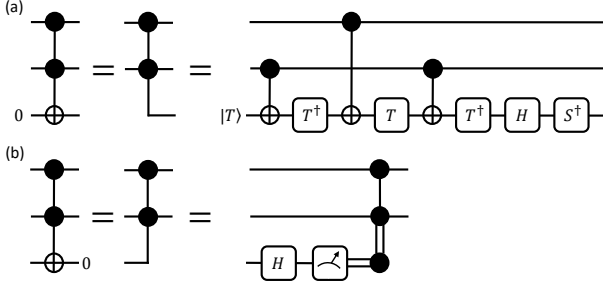


FIG. 23. **Elbows** In (a), a compilation scheme for a Toffoli gate acting on a clean ancillae is shown that uses four  $T$  gates. This is sometimes referred to as a “left-elbow”. In (b), a compilation scheme for a Toffoli gate that uncomputes a clean ancillae is shown that uses a measurement and classically conditioned operation. This is sometimes referred to as a “right-elbow”.

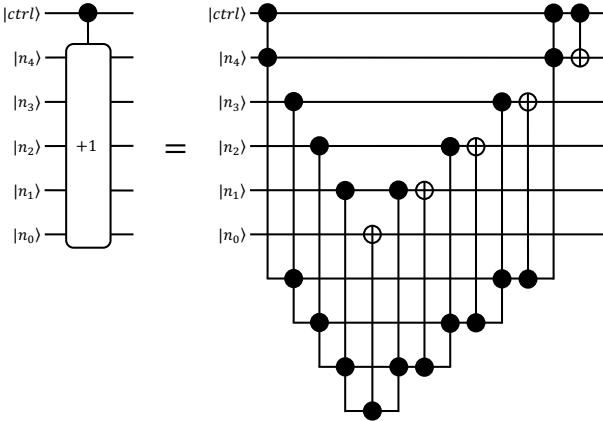


FIG. 24. **Controlled Incrementer** A circuit diagram implementing a controlled incrementer (mod 32) is shown. The controlled incrementer performs the operation  $|x\rangle \rightarrow |x + 1\rangle$  when the control qubit is in the  $|1\rangle$  state. Decrementing the register by 1 can be achieved by applying Pauli-X gates on each qubit before and after the operation.

Another implementation can be chosen to reduce the number of clean ancillae, which uses the classical information about  $m$  to modify the circuit for *controlled* quantum addition. Controlled addition of two registers can be performed using  $4(2N - 3)$   $T$  gates and  $2N - 1$  clean ancil-

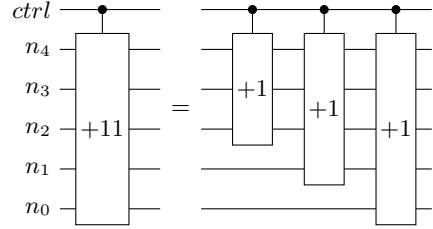


FIG. 25. **Addition via Incrementers** An implementation of addition by a classical value (11) (mod 32) using a series of incrementers is shown. An incrementer applied onto a register excluding the least-significant qubit implements a bit-shifted incrementer. This effectively increases the value of the register by 2. Addition by the classical value 11 can be constructed by bit-shifted incrementers adding the values +8, +2, and +1. Subtraction by the same value can be achieved by applying Pauli-X gates on each qubit before and after the operation.

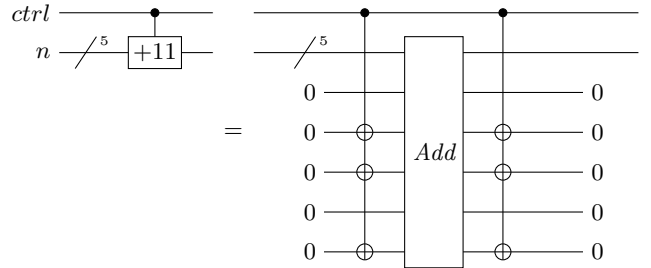


FIG. 26. **Time-Efficient Controlled Addition of 11** Increasing the value of a quantum register by a known classical value can be implemented using clean ancillae and an uncontrolled quantum addition circuit. The known classical value is loaded into a clean ancilla register using a series of CNOT gates corresponding to the binary representation of the classical value. Then an uncontrolled quantum addition circuit is applied to the two registers. Finally, the loading of the classical value is uncomputed.

lae using the construction for addition shown in Figure 4 of [70]. This circuit can be modified by propagating the classical information about the binary encoding of  $m$  into the control structure of the adder circuit, thereby reducing the number of clean ancillae by  $N$ . An example diagram showing this propagation in the case where  $m = 11$  and  $N = 5$  is shown in Figure 27.

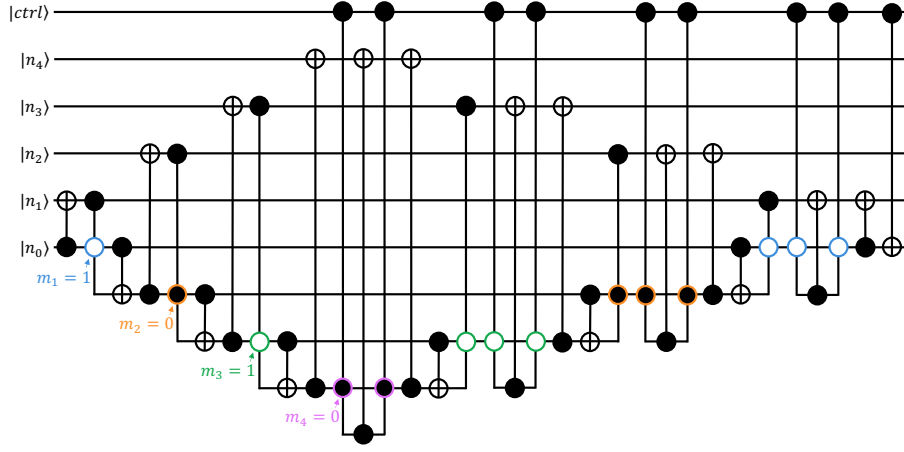


FIG. 27. **Space-Efficient Controlled Addition of 11** An implementation for increasing the value of a register by a known classical value is shown for the case when the known value is 11 and the number of qubits in the register is 5. The binary representation of 11 is 01011 with the left-most bit being the most-significant. The values of these  $M$  classical bits can be propagated into the control structure of the controlled quantum addition. If the value of the  $i^{\text{th}}$  bit of  $M$  is 0 (1), the corresponding control in the circuit is controlled on the  $|1\rangle$  ( $|0\rangle$ ) state.

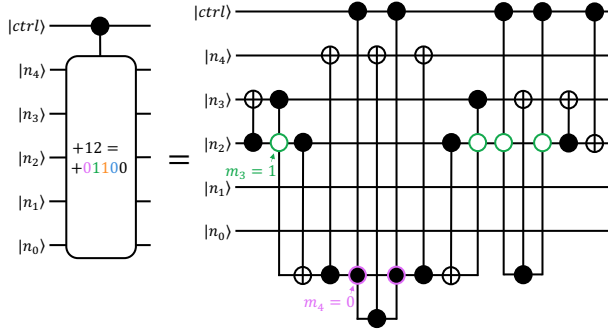


FIG. 28. **Space-Efficient Controlled Addition of 12** An implementation for increasing the value of a register by a known classical value is shown for the case when the known value is 12 (01100 in binary) and the number of qubits in the register is 5. When the least-significant bits of  $M$  are 0, the circuit can be bit-shifted, resulting in a lower cost implementation. In this case, the two least-significant bits are 0, so the circuit can be bit-shifted twice.

Similarly, if the  $p$  least-significant bits of  $m$  are known to be zero, the addition can be performed beginning with the first non-zero bit of  $m$ . An example circuit diagram for the case where  $m = 12$  (01100 in binary) and  $N = 5$  is shown in Figure 28. If the  $p$  least significant bits of  $m$  are zero, then this circuit uses  $4(2(N - p) - 3)$   $T$  gates and  $N - p - 1$  clean ancillae. Since this work primarily focuses on reducing the number of  $T$  gates, the quantum resource estimates quoted in this work do not utilize this strategy.

## Appendix E: Pauli Expansion of Fermionic and Bosonic Ladder Operators

In this Section, we review the two different operator transformations that are used in this work to express the ladder operators in the Pauli basis.

### 1. Jordan-Wigner Transformation

The fermionic ladder operators are mapped under the *Jordan-Wigner (JW)* [46] transform. These operators increase or decrease the occupation number of the fermionic state by 1 for creation and annihilation operators respectively. The corresponding qubit operator that accomplishes this on a given mode (qubit) is given by  $\frac{1}{2}(X \mp iY)_i$  for creation ( $-$ ) and annihilation ( $+$ ) operators on mode  $i$ . This is not the entire transformation; however, because it does not pick up the property parity exchange rules for fermions. A string of Pauli  $Z$ 's are included on qubits less than the mode being acted on to satisfy this requirement.

The full mapping from ladder operator  $\rightarrow$  Pauli operator is:

$$b_i = \frac{1}{2}(X_i + iY_i) \otimes Z_{i-1} \otimes \cdots \otimes Z_0 \quad (\text{E1})$$

$$b_i^\dagger = \frac{1}{2}(X_i - iY_i) \otimes Z_{i-1} \otimes \cdots \otimes Z_0 \quad (\text{E2})$$

Identities may be tensored on for any mode  $j > i$  if necessary.

## 2. Standard Binary

In this work, the registers encoding the occupation of the bosonic modes store the value of the occupation in binary notation. The Standard Binary encoding [50] provides a method for expanding the bosonic ladder operators in the Pauli basis when this binary encoding is used.

The expansion in the Pauli basis begins by noting the following definitions of the bosonic creation and annihilation operators:

$$a^\dagger = \sum_{s=0}^{\Omega-1} \sqrt{s+1} |s+1\rangle \langle s| = |1\rangle \langle 0| + \sqrt{2} |2\rangle \langle 1| + \dots \quad (\text{E3})$$

$$a = \sum_{s=0}^{\Omega-1} \sqrt{s+1} |s\rangle \langle s+1| = |0\rangle \langle 1| + \sqrt{2} |1\rangle \langle 2| + \dots \quad (\text{E4})$$

$$(\text{E5})$$

From here, each state in the expansion of  $a$  and  $a^\dagger$  is converted into binary, e.g.  $|3\rangle = |0\dots 011\rangle$ , where the preceding (most-significant) qubits are zeros and the total length of the register is given by  $\lceil \log_2(\Omega+1) \rceil$ .

Now, each outer product in Eq. E3 can be expanded by computing the outer product of the individual qubit values tensored together. For example, with  $\Omega = 3$  the outer product of  $|2\rangle$  and  $|3\rangle$  is given by:

$$|2\rangle \langle 3| = |10\rangle \langle 11| = |1\rangle \langle 1| \otimes |0\rangle \langle 0|. \quad (\text{E6})$$

Each single-qubit outer product can be mapped onto the Pauli basis using the following relations:

$$|0\rangle \langle 0| = \frac{1}{2} (I + Z) \quad (\text{E7})$$

$$|0\rangle \langle 1| = \frac{1}{2} (X + iY) \quad (\text{E8})$$

$$|1\rangle \langle 0| = \frac{1}{2} (X - iY) \quad (\text{E9})$$

$$|1\rangle \langle 1| = \frac{1}{2} (I - Z) \quad (\text{E10})$$

$$(\text{E11})$$

Finally, these single-qubit outer products can be tensored together to give the expansion of the multi-qubit outer products, thereby representing the ladder operators as a linear combination of Pauli operators.

An explicit example with  $\Omega = 3$  is shown below:

$$a_0^\dagger = 0.683IX - 0.183ZX - 0.683iY \quad (\text{E12})$$

$$+ 0.183iZY + 0.354XX - 0.354iYX \quad (\text{E13})$$

$$+ 0.354iXY + 0.354YY \quad (\text{E14})$$

### Appendix F: Uniformly Controlled Rotations

Implementing a series of uniformly controlled rotations is a common subroutine used in this work. In this Sec-

tion, we discuss the cost and explicit circuit compilation for a series of uniformly controlled rotations around the same axis (but different angles) are applied on the same qubit:

$$\sum_{l=0}^{L-1} |l\rangle \langle \phi| \rightarrow \sum_{l=0}^{L-1} |l\rangle R_a(\alpha_l) |\phi\rangle \quad (\text{F1})$$

Möttönen et. al [69], provide a construction for *uncontrolled* uniformly controlled rotations. This construction is only defined when the number of rotations ( $L$ ) is explicitly a power of 2, however, if fewer rotations are required, then this can be achieved by padding with zero-angle rotations.

In this construction, the rotation angles are classically preprocessed based on the Gray code (Eq. 3 of [69]):

$$\begin{bmatrix} \theta_0 \\ \theta_1 \\ \vdots \\ \theta_{L-1} \end{bmatrix} = M \begin{bmatrix} \alpha_0 \\ \alpha_1 \\ \vdots \\ \alpha_{L-1} \end{bmatrix} \quad (\text{F2})$$

where  $M$  is a matrix transformation defined by:

$$M_{i,j} = L^{-1} (-1)^{b_j \cdot g_i} \quad (\text{F3})$$

where  $b_j$  is the binary representation of the integer  $j$ ,  $g_i$  is the Gray code representation of the integer  $i$ , and  $b_j \cdot g_i$  is the bitwise inner product of  $b_j$  and  $g_i$ .

However, in this work we require the use of a *controlled* series of uniformly controlled rotations. Naively, this can be implemented by controlling each of the arbitrary rotations in the construction given by Möttönen et al. [69]. An example circuit diagram for this construction is shown in Subfigure 29a. Since each controlled rotation can be implemented by two uncontrolled rotations, this compilation strategy uses  $2L$  uncontrolled arbitrary rotations.

An alternative approach which uses  $4 \log_2 L$  T gates,  $L + 3$  arbitrary rotations, and  $\log_2 L$  clean ancillae is shown in Subfigure 29b. In this construction, the temporary logical-AND of each qubit in the index register and the control qubit is computed using  $\log_2 L$  Toffoli gates. CNOTs from these clean ancillae then conjugate each of the arbitrary rotations which are left uncontrolled. When the control is on, this fully recovers the construction given by Möttönen et. al.

However, when the control is off, the uncontrolled arbitrary rotations are still applied, resulting an undesired rotation of angle  $\sum_i(\theta_i)$ . This undesired rotation can then be undone using one 0-controlled rotation of angle  $-\sum_i(\theta_i)$ .

### Appendix G: Grover-Rudolph State Preparation

In this Section, we will describe the Grover-Rudolph state preparation routine [63] in the context that it is

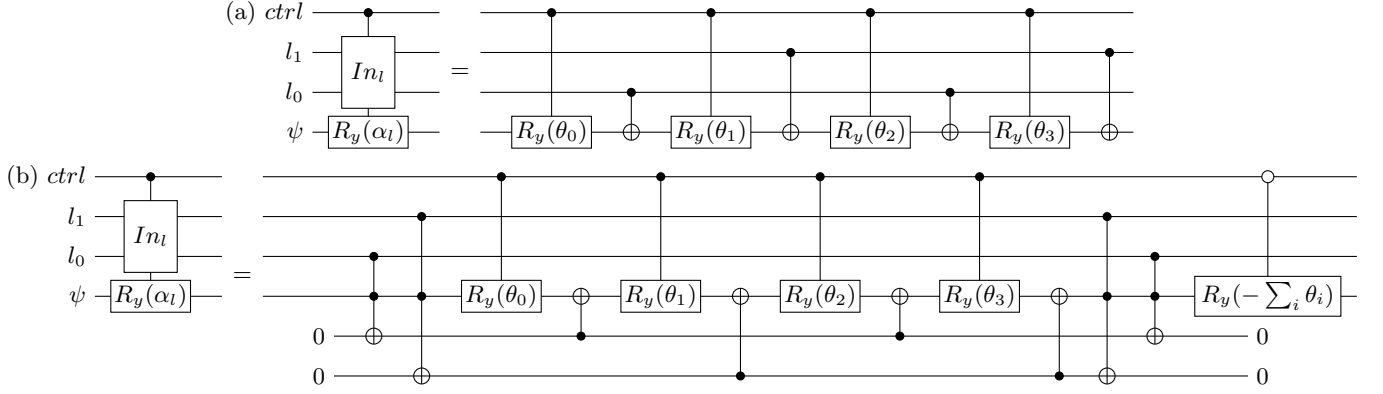


FIG. 29. **Controlled Uniformly Controlled Rotations** Two implementations for controlling a series of uniformly controlled rotations are shown. In (a), a naive implementation is shown which doubles the number of arbitrary rotations required. The implementation shown in (b) uses only one additional controlled rotation and  $\log_2 L$  Toffoli gates, but requires  $\log_2 L$  clean ancillae.

used in this work. The Grover-Rudolph state preparation algorithm constructs quantum circuits that prepare states of the form given by:

$$|0^{\otimes \lceil \log_2 L \rceil}\rangle \rightarrow_{\text{Grover-Rudolph}} \sum_{l=0}^L \sqrt{p(l)} |l\rangle \quad (\text{G1})$$

where  $p(l)$  is a probability distribution along the different indices ( $l$ ) with the constraint that  $\sum_l p(l) = 1$ .

In the context of block-encodings, preparing such probability distributions can be used to construct the *Prepare* oracle (Eq. 19). The probability distribution in this case is defined by the normalized magnitudes of the coefficients of the terms in the linear combination:  $p(l) = |\alpha_l|/\lambda$ .

The Grover-Rudolph algorithm works by sequentially summing up the probability distribution to the left and right of a given index and then performing a rotation controlled on the current index.

For example, given the (normalized) probabilities  $\alpha_0$ ,  $\alpha_1$ ,  $\alpha_2$ , and  $\alpha_3$ , the Grover-Rudolph algorithm proceeds as follows:

1. Perform a Pauli-Y rotation on the top (left-most) qubit in the register by an angle:  $\theta = 2 \cos^{-1}(\sqrt{\alpha_0 + \alpha_1})$ .
2. Perform a Pauli-Y rotation on the second qubit in the register, controlled on the first qubit being in the state  $|0\rangle$  by an angle:  $\theta = 2 \cos^{-1}(\sqrt{\frac{\alpha_0}{\alpha_0 + \alpha_1}})$
3. Perform a Pauli-Y rotation on the second qubit in the register, controlled on the first qubit being in the state  $|1\rangle$  by an angle:  $\theta = 2 \cos^{-1}(\sqrt{\frac{\alpha_2}{\alpha_2 + \alpha_3}})$

The evolution of the quantum state is given by:

$$\begin{aligned} |00\rangle &\rightarrow_{(i)} \sqrt{\alpha_0 + \alpha_1} |00\rangle + \sqrt{\alpha_2 + \alpha_3} |10\rangle \\ &\rightarrow_{(ii)} \sqrt{\alpha_0} |00\rangle + \sqrt{\alpha_1} |01\rangle + \sqrt{\alpha_2 + \alpha_3} |10\rangle \\ &\rightarrow_{(iii)} \sqrt{\alpha_0} |00\rangle + \sqrt{\alpha_1} |01\rangle + \sqrt{\alpha_2} |10\rangle + \sqrt{\alpha_3} |11\rangle \end{aligned} \quad (\text{G2})$$

The Grover-Rudolph algorithm can be thought of as performing several series of uniformly controlled rotations. An example circuit diagram depicting this construction is shown in Figure 30. When  $L$  is the number of probabilities (or coefficients) to prepare and is a power of 2, this implementation uses  $L - 1$  uncontrolled rotations.

## Appendix H: Quantum Field Theory Hamiltonians

The two quantum field theory models studied in Section V are the  $\phi^4$  and Yukawa model. In performing a Legendre transformation from the Lagrangian to the Hamiltonian,  $\mathcal{L} \rightarrow H$ , one must choose an explicit coordinate system. Any field theory calculation done in a Hamiltonian approach benefits from using *front form* (light front) coordinates [86]. Lightfront coordinates are defined as  $x^\mu = (x^+, x^-, x^1, x^2)$ , where  $x^+ \equiv x^0 + x^3$  acts as the space coordinate and  $x^- \equiv x^0 - x^3$  acts as the time coordinate. In each model studied above, the transverse spatial coordinates  $x^1, x^2$  are discarded, and the only independent coordinates are  $x^+$  and  $x^-$ .

One main benefit of using this set of coordinates is that the Hamiltonian eigenvalue equation, whose eigenvectors are bound states of the theory, is simpler than in instant (equal time) coordinates. This is because the Hamiltonian operator in instant form coordinates is  $H = \sqrt{\vec{P}^2 + m^2}$ , where the presence of the square root leads to an ambiguity. In front form coordinates, the

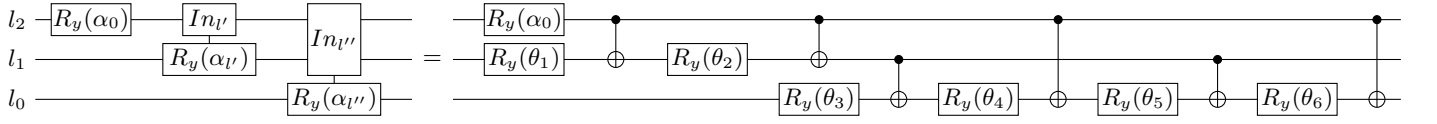


FIG. 30. **Grover-Rudolph Circuit Compilation.** An implementation of the Grover-Rudolph algorithm using several series of uniformly controlled rotations is shown when  $L = 8$ . This circuit requires  $L - 1$  rotations when  $L$  is a power of 2 and the angles of the rotations are changed ( $\theta_i \rightarrow \alpha_i$ ) based on classical preprocessing.

Hamiltonian operator is given via the quantized light-front ‘energy’

$$\hat{P}^- = \frac{(\vec{P}^\perp)^2 + m^2}{P^+},$$

where the square root is absent.

In one light front space and time dimension, the Hamiltonian eigenvalue equation is given by  $\hat{P}^-|\psi\rangle = \frac{m^2}{P^+}|\psi\rangle$ . Any state can be expanded as

$$|\psi\rangle = \sum_n \int d[\mu_n] |\mu_n\rangle \langle \mu_n | \psi \rangle,$$

where  $\{|\mu_n\rangle\}$  is a set of Fock states with  $n$  particles, i.e.  $|f\rangle, |ff\rangle, |b\rangle, |fb\rangle, \dots$

The light front ‘momentum’  $P^+$  is a conserved quantity which every constituent’s longitudinal momentum in a given Fock state  $\in \{|\mu_n\rangle\}$  must sum to  $P^+$ . The ‘modes’ of the ladder operators correspond to discrete longitudinal momentum quantum numbers  $k$ , where the discretized approximation to a continuous constituent momentum  $p^+ = \frac{\pi k}{L}$ , where  $L$  truncates  $x^-$  to a finite region. Thus, the conservation of  $P^+$  is analogous to  $\sum k = K$ , labeled the *resolution* [74]. Increasing the resolution leads to a larger Hilbert space of states, with a more refined set of momentum values these states can describe, and thus the number of terms in the Hamiltonian that act non-trivially on this set of states also expands. This is why increasing  $K$  is a metric for ‘number of terms in the Hamiltonian’.